

Review

A Critical Review on Recent Advancements in Aluminium-Based Metal Matrix Composites

Amlan Kar ^{1,*} , Aditya Sharma ² and Sachin Kumar ^{3,*}

¹ Arbogast Materials Processing and Joining Laboratory, South Dakota, School of Mines & Technology, Rapid City, SD 57701, USA

² Department of Mechanical Engineering, Faculty of Engineering, Dayalbagh Educational Institute, Dayalbagh, Agra 282005, Uttar Pradesh, India; adityasharma@dei.ac.in

³ Department of Mechanical Engineering, PDPM-Indian Institute of Information Technology, Design and Manufacturing (IIITDM), Jabalpur 482005, Madhya Pradesh, India

* Correspondence: amlan.kar@sdsmt.edu (A.K.); sachink@iiitdmj.ac.in (S.K.)

Abstract: Aluminum matrix composites (AMCs) have garnered significant attention across various industrial sectors owing to their remarkable properties compared to conventional engineering materials. These include low density, high strength-to-weight ratio, excellent corrosion resistance, enhanced wear resistance, and favorable high-temperature properties. These materials find extensive applications in the military, automotive, and aerospace industries. AMCs are manufactured using diverse processing techniques, tailored to their specific classifications. Over three decades of intensive research have yielded numerous scientific revelations regarding the internal and extrinsic influences of ceramic reinforcement on the mechanical, thermomechanical, tribological, and physical characteristics of AMCs. In recent times, AMCs have witnessed a surge in usage across high-tech structural and functional domains, encompassing sports and recreation, automotive, aerospace, defense, and thermal management applications. Notably, studies on particle-reinforced cast AMCs originated in India during the 1970s, attained industrial maturity in developed nations, and are now progressively penetrating the mainstream materials arena. This study provides a comprehensive understanding of AMC material systems, encompassing processing, microstructure, characteristics, and applications, with the latest advancements in the field.



Citation: Kar, A.; Sharma, A.; Kumar, S. A Critical Review on Recent Advancements in Aluminium-Based Metal Matrix Composites. *Crystals* **2024**, *14*, 412. <https://doi.org/10.3390/cryst14050412>

Academic Editor: Umberto Prisco

Received: 29 March 2024

Revised: 15 April 2024

Accepted: 25 April 2024

Published: 28 April 2024



Copyright: © 2024 by the authors. Licensee MDPI, Basel, Switzerland. This article is an open access article distributed under the terms and conditions of the Creative Commons Attribution (CC BY) license (<https://creativecommons.org/licenses/by/4.0/>).

Keywords: powder metallurgy; stir casting; mechanical behavior; diffusion bonding; direct energy deposition; cold spraying

1. Introduction

The growth of Al-based metal matrix composites (AMCs) was motivated by the need for lightweight, high-performance engineered materials in automotive, transportation, and defense applications. Because of their enhanced mechanical and physical characteristics and the creation of a substitute for obtaining materials with high stiffness, AMC demand has increased several-fold in the last 20 years. AMCs, due to their astonishing characteristics, such as high toughness, low density, and corrosion resistance [1], have become an ideal candidate for aerospace, military, automotive, and mineral processing sectors. Alumina oxide (Al₂O₃) and silicon carbide (SiC) are reinforcing materials that are frequently utilized in automotive applications, including drive shafts, braking discs, cylinder liners, pistons, rings, and connecting rods [2]. Al₂O₃ is a commonly utilized reinforcement that exhibits superior corrosion and high-temperature resistance, following SiC. The difficult task in manufacturing reinforced AMCs is ensuring uniform dispersion of reinforced particles without agglomeration and the least interfacial reactions [3]. Composite materials, such as polymer matrix, metal matrix, and ceramic composites, are often categorized based on the physical or chemical characteristics of the matrix phase [4].

Furthermore, some data suggest that carbon matrix and intermetallic matrix composites are starting to appear. One of the components of AMCs is aluminum alloy, referred to as matrix phase, which forms a percolating network. The other component, typically non-metallic and frequently ceramic (SiC and Al₂O₃), is incorporated in this aluminum matrix and acts as reinforcement. AMCs' properties can be customized by changing the composition and volume percentage of their elements [4].

When compared to unreinforced materials, the following are AMCs' main advantages:

- Increased strength;
- Enhanced stiffness;
- Decreased density (weight);
- Enhanced properties at high temperatures;
- Regulated thermal expansion coefficient;
- Thermal and heat management;
- Superior and customized electrical characteristics;
- Better abrasion and wear resistance;
- Mass control (particularly in reciprocating applications);
- Enhanced damping properties.

For a better understanding, these benefits might be put into numbers. For instance, by adding 60 vol.% continuous Al fiber for reinforcement, the elastic modulus of pure Al can be improved from 70 GPa to 240 GPa. Conversely, adding 60% alumina fiber to pure aluminum causes the coefficient of expansion to drop from 24 ppm = °C to 7 ppm = °C. Similarly, Al-9% Si-20 vol.% SiC_p composites with wear resistance comparable to or better to grey cast iron can be processed. These examples all show how adding the right reinforcement to the right volume fraction can change a number of the technological attributes of Al and its alloy by more than two or three orders of magnitude.

AMC's material systems provide a better profile of qualities in combination that are currently unmatched by any monolithic material on the market. AMCs have been incorporated in many structural, non-structural, and functional domains across several engineering applications over the years. The use of AMCs in these industries is motivated by performance, economy, and environmental advantages. Reduced noise, reduced fuel consumption, and less airborne pollution are the main advantages of AMCs in the transportation industry. In the upcoming years, the usage of AMCs in the transportation industry will be both necessary and desired due to tighter environmental restrictions and an emphasis on increased fuel economy.

In a variety of applications, AMCs are meant to replace monolithic materials such as polymer-based composites, ferrous alloys, titanium alloys, and aluminum alloys. It is now understood that a complete system redesign is necessary to achieve significant weight and volume savings before AMCs—which replace monolithic materials in engineering systems—can be widely adopted. In reality, the UK Advisory Council on Science and Technology states that AMCs can be used to enable significant modifications to system or product design, or they might be seen as an improved alternative to current materials. Additionally, by employing selective reinforcing and near-net shape-forming processes, AMCs can provide commercially feasible solutions for a broad range of applications.

These creative design modifications to the component are partially responsible for the recent success of AMCs in both commercial and military applications. The full-fledged application of AMCs has been restricted owing lack of understanding and information on utilization possibilities, service attributes, and material producers. The AMC community in the USA and Europe is seeking consortium and networking ways for integrating AMC applications into regular societal use, acknowledging these auxiliary and extraneous challenges. An overview of the state of the art for AMCs, including production, microstructure, characteristics, and applications, is provided in this article. There are also opportunities and challenges for the extensive usage of AMCs.

2. Classification of AMCs

AMCs can be in the following categories, depending on the forms of reinforcement (Figure 1).

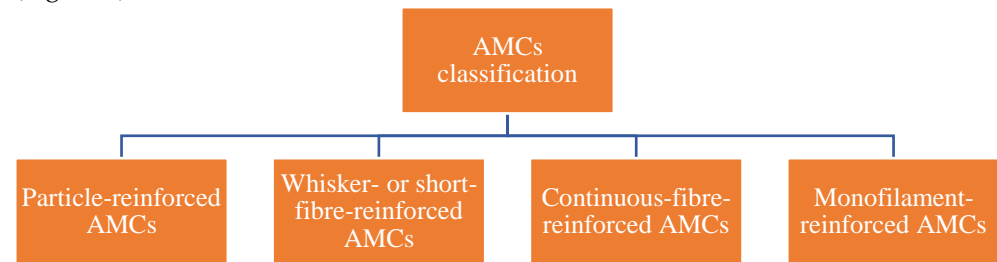


Figure 1. Typical classification of AMCs.

2.1. Particle Reinforced Aluminium Matrix Composites

Equiaxed ceramic reinforcements with an aspect ratio of less than or equal to five are typically present in these composites. For structural and wear resistance purposes, ceramic reinforcements are often oxides, carbides, or borides (Al_2O_3 , SiC , or TiB_2) with a volume fraction of less than 30%. However, the reinforcement volume fraction may reach 70% in electronic packaging applications. Generally speaking, there are two ways to make PAMCs: liquid state (stir casting, infiltration, and in situ) or solid state (PM processing) [5,6]. When it comes to cost, PAMCs cost less than CFAMCs. The mechanical characteristics of PAMCs are significantly better than those of unreinforced aluminum alloys, although they are not as good as those of whisker, short fiber, or continuous-fiber-reinforced AMCs [6]. These composites can undergo a range of secondary forming processes, such as extrusion, rolling, and forging, and are isotropic in nature. Particle addition increases the hardness, yield strength, tensile strength, wear resistance, and Young's modulus of light metals like aluminum while decreasing the thermal expansion coefficient [5].

2.2. Whisker- or Short-Fibre-Reinforced AMCs

These are not continuous, although they contain reinforcements with an aspect ratio larger than 5. One of the earliest and most well-known AMCs to be created and utilized in pistons is short-alumina-fiber-reinforced AMCs. These were created using squeezing infiltration. Composites reinforced with whiskers can be made using infiltration or PM processing. When compared to particle- or short-fiber-reinforced composites, whisker-reinforced composites have better mechanical characteristics. However, because of the perceived health risks, the use of whiskers as reinforcements in AMCs has decreased recently. As a result, there has been relatively little commercial use of whisker-reinforced composites. AMCs reinforced with short fibers exhibit properties halfway between those of continuous fiber and particle reinforcement.

2.3. Continuous-Fibre-Reinforced AMCs

In this instance, the reinforcements take the shape of continuous fibers with a diameter of less than $20\ \mu\text{m}$ made of carbon, SiC , or alumina. Prior to the composite's creation, the fibers might be braided or prewoven in parallel. Squeeze infiltration is the process used to create AMCs with a fiber volume fraction of up to 40% [6]. In recent times, the 3MTm Corporation has created a composite reinforced with 60% alumina fiber (continuous fiber) that exhibits tensile strength and elastic stiffness of 1500 MPa and 240 GPa, respectively. Pressure infiltration is the process used to create these composites.

2.4. Monofilament-Reinforced AMCs

Large-diameter (100 to $150\ \mu\text{m}$) fibers known as monofilaments are often created by chemical vapor deposition of SiC or B into a carbon fiber or W wire core. In comparison to multifilaments, monofilaments have less bending flexibility. Diffusion bonding techniques are in common to create monofilament-reinforced AMCs, which are only possible with

superplastic-forming aluminum alloy matrices. The primary load-bearing component in CFAMCs and MFAMCs is the reinforcement, and the aluminum matrix’s function is to link the reinforcement while transferring and distributing the load. There is directionality in these composites. CFAMCs and MFAMCs are characterized by low strength in the direction perpendicular to the fiber orientation. The primary component of AMCs reinforced with particles and whiskers that bear the load is the matrix. Through mechanical restraint, the reinforcement’s function is to prevent matrix deformation and strengthen and stiffen the composite. Apart from the four categories of AMCs mentioned above, hybrid AMCs are a newly designed variety that are partially utilized. In essence, hybrid AMCs have many reinforcing types. As an illustration, consider combinations of whisker and particle, fiber and particle, or hard and soft reinforcements. A hybrid composite is an aluminum matrix composite that is utilized in cylindrical liner applications and contains a blend of carbon fiber and alumina particles.

3. Major AMC Manufacturing Techniques

The manufacturing process used to create any composite is crucial in establishing the material’s final characteristics [7]. A multitude of methodologies are being employed in the process of creating high-grade MMC products. As illustrated in Figure 2, the primary techniques for producing AMCs on an industrial scale can be categorized into three major domains:

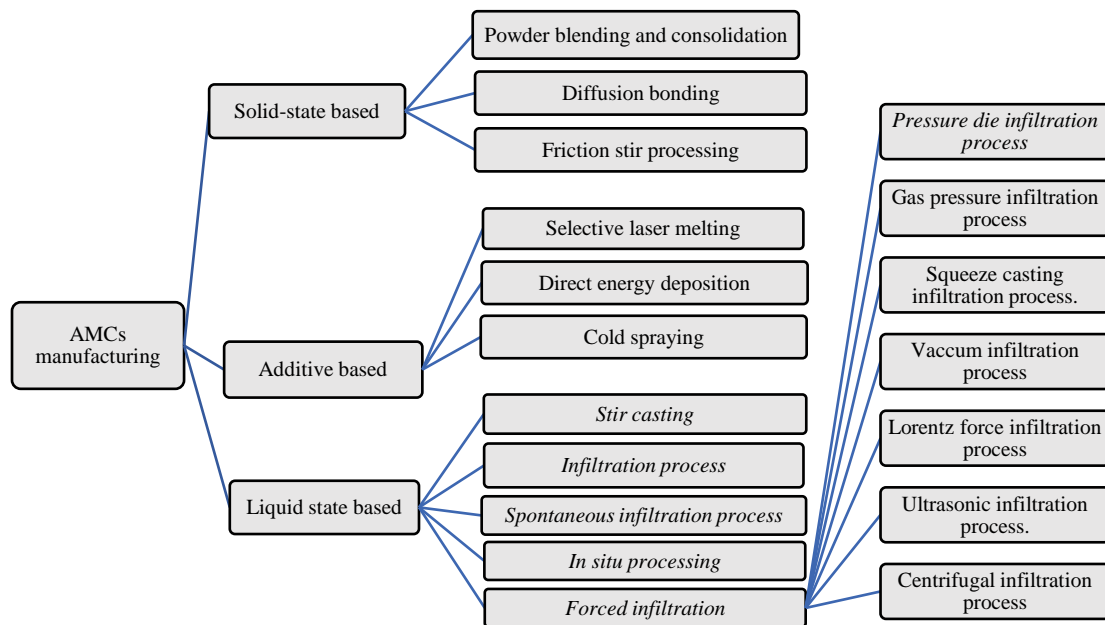


Figure 2. AMCs manufacturing techniques.

Figure 3 highlights commonly employed metal matrix composite production techniques. Table 1 lists the key components of several techniques for manufacturing MMCs and discusses them. Agglomeration and dendritic segregation are the primary problems with liquid phase procedures; they arise from the uneven spread of ceramic particles in the metallic matrix and unfavorable chemical reactions at the interface brought on by the melt’s high temperature. Table 2 lists the various MMC processing routes, their associated costs, and their applications. It demonstrates that the best technique for creating MMCs is powder metallurgy since there are no interfacial interactions between the reinforcement and matrix.

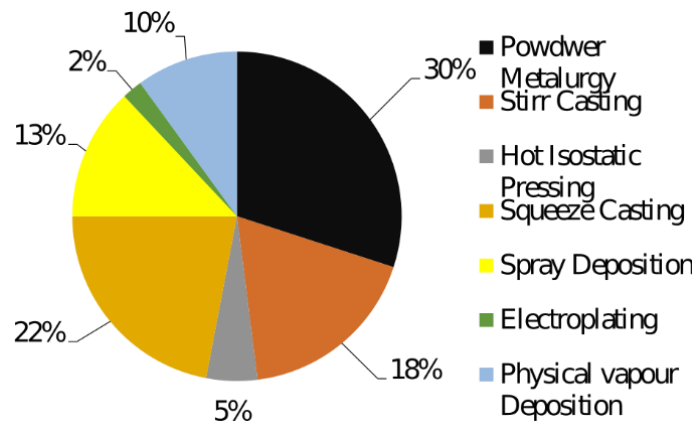


Figure 3. MMCs fabrication route share by percentage [8].

Table 1. MMCs fabrication categories [8].

Composite Type/Process	Examples (Reinforcement/Matrix)	Main Features
Solid-state processing		
In situ forming-internal oxidation	Al ₂ O ₃ /SiO ₂ BeO particulate in Cu or Ag	Good electrical conductivity, modest strength increase
Powder forming		
Sintered aluminum powder	Al ₂ O ₃ particulate/Al matrix	Moderate strength and stiffness around 300 °C, Low density
Long or short fibers or particulates incorporated by powder metallurgy		Good stiffness/strength to modest particulate incorporated temperatures, Low density, Low thermal expansion
Mechanical alloying	Oxide particles in super alloy matrix	High-performance alloy, High strength at high temperatures
Diffusion bonding		
Long fibers in intermetallic	SiC fibers in Ti ₃ Al, etc.	Some problems over oxidation at high temperatures
Liquid state processing		
Molten metal mix processing	SiC or Al ₂ O ₃ /Light alloy matrices	Modest improvements in properties
Infiltration of preforms	SiC whiskers, Al ₂ O ₃ fibers/Al alloys C/Al and Mg alloys SiC/Ti alloys B/Al alloys	Good stiffness and strength to 200 °C, Low density, Low thermal conductivity
Dispersion semi solidus processing	Various ceramic dispersoids into the melt Si in Al	Some problems in controlling the microstructure, Modest strength
Spraying	Particulate/short or long fibers in alloy matrices, for example, Sic or Al ₂ O ₃ in Al alloys	Good wear characteristics, Good stiffness and strength, Low density, Low thermal expansion coefficient
In situ processing	TiB ₂ particulate/Al alloy	Good strength ductility and toughness, Fatigue resistant
Other techniques		
Molecular level mixing	Carbon nanotubes (CNTs) reinforced copper (Cu) matrix nano composites	No clustering of molecules Uniform dispersion
CIP + HIP	TiCp particulate/Al alloy	Formation of oxidation constraint of high-temperature use, Microstructure modification
Sputtering method	Titanium aluminide alloy, Ti–Al–Nb, on short length Sic fibers	Clean environment with excellent impurity control, Good repeatability/reproducibility, Homogeneity of the deposited matrix

Table 2. Comparison of MMC techniques [9,10].

Route	Cost	Applications	Comments
Diffusion bonding	High	Used to make sheets, blades, vane shafts, structural components	Handles foils or sheets of matrix and filaments of reinforcing elements
Powder metallurgy	Medium	Mainly used to produce small objects (especially round), bolts, valves, high-strength and heat-resistant materials	Both matrix and reinforcements used in powder form, best for particulate reinforcement. Since no melting is involved, no reaction zone is developed, showing a high-strength composite
Liquid-metal infiltration	Low/medium	Used to produce structural shapes such as rods, tubes, and beams with maximum properties in a uniaxial direction	Filaments of reinforcement used
Squeeze casting	Medium	Widely used in the automotive industry for producing different components such as pistons, connecting rods, rocker arms, and cylinder heads suitable for making complex objects	Generally applicable to any type of reinforcement and may be used for large-scale manufacturing
Spray casting	Medium	Used to produce friction materials, electrical brushes and contacts, cutting and grinding tools	Particulate reinforcement used: full-density materials can be produced
Compcasting/Rheocasting	Low	Widely used in automotive, aerospace, industrial equipment and sporting goods industries, used to manufacture bearing materials	Particulate reinforcement used: full-density materials can be produced. Suitable for discontinuous fibers especially particulate reinforcement

3.1. Solid-State-Based Techniques

3.1.1. Powder Blending and Consolidation (P/M Processing)

Since powder metallurgy makes it simple to create composites with high weight percentages of reinforcements, it is a crucial technology in the development of binary and hybrid AMCs [11]. Furthermore, using this technique, hybrid AMCs with nanoparticle reinforcement can also be created [12]. The reason for its amazing growth is that this method was created, refined, and utilized in conventional metallurgy before being modified for use in metal matrix composites [7]. For the creation of AMCs, blending powdered aluminum alloy with ceramic short fiber or whisker particles is a flexible method. You can blend in a liquid suspension or on its own. Cold compaction, canning, degassing, and high-temperature consolidation stages like hot isostatic pressing (HIP) or extrusion typically come after blending. Reliant on the powder history and processing circumstances, PM-processed AMCs are found to have oxide particles in the volume fraction range of 0.05 to 0.5, resembling plates with a thickness of a few tens of nm. These tiny oxide particles may cast a major influence on the matrix, especially after heat treatment, and have a tendency to operate as a dispersion-strengthening agent.

The necessary and particular steps for processing powder metallurgy composites are depicted in Figure 4.

PM structural part production is manufactured using either the sponge iron process or water atomization.

Powder mixing is followed by the introduction of alloying additions in elemental powder form or the incorporation of a pressing lubricant.

Compaction is the pressing in a rigid toolset, comprising a die, punches and, possibly, mandrels or core rods.

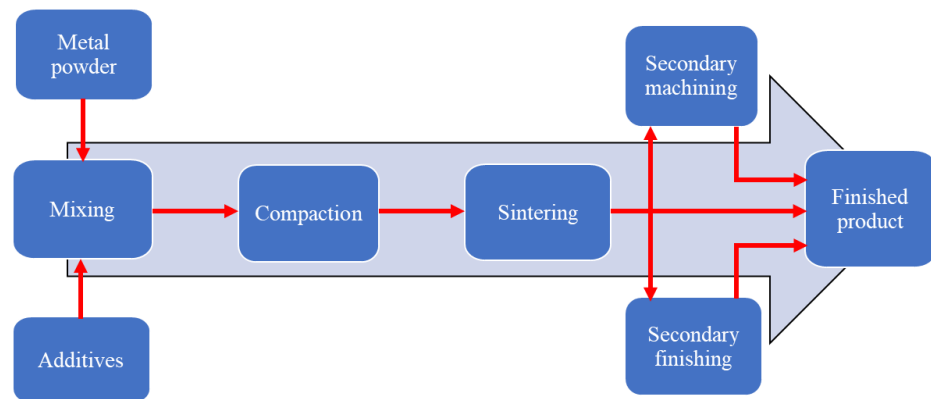


Figure 4. Steps involved in Powder Metallurgy.

Sintering involves heating the material, usually in a protective atmosphere, to a temperature that is below the melting point of the major constituent.

Secondary operations are optional, and may or may not be required based on end requirement.

Figure 5a,b depicts a matrix having a homogeneous spread of reinforced particles, whereas in Figure 5c,d clustering of reinforcing agent is clearly seen which may be because of high particle size ratios [13,14]. The clustering of SiC particles occurs across bigger Al alloy particles when the particle size ratio increases because of the small combined surface area of the reinforcement and matrix particles.

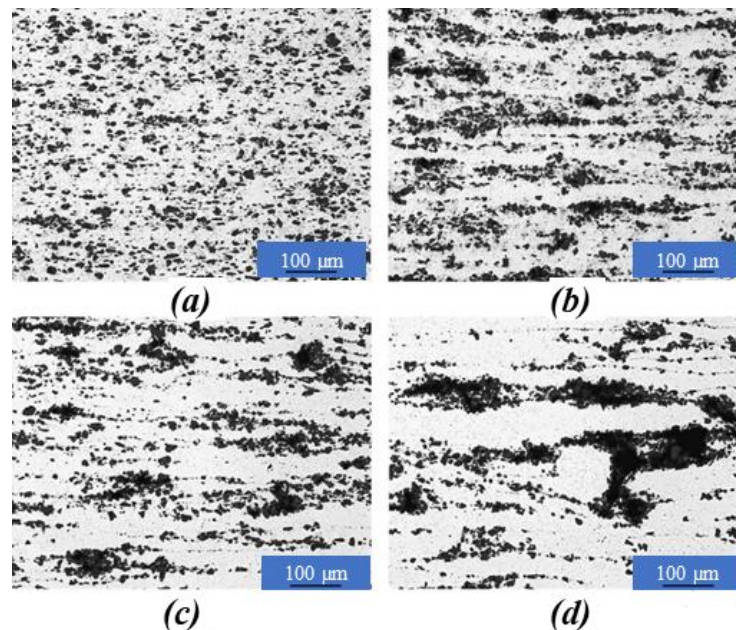


Figure 5. Composite reinforcement using prepared powders (Al–6 wt.% Cu–0.4 wt.% Mn matrix alloy reinforced with SiC particulate) of particle size ratios. (a) 2.9; (b) 5.7; (c) 9.3; (d) 12.9 [13].

3.1.2. Diffusion Bonding

Diffusion bonding is a technique, used to combine materials that are similar or dissimilar, mostly metals; however, ceramic materials can also be linked using this method. The mechanism is based on the high-temperature diffusion of atoms over the joint interface. Usually, it is carried out at a temperature that is higher than 50–75% of the materials' absolute melting points. The diffusion forming, especially for common long composite fiber, involves applying high temperatures and pressure mechanically to create a process that securely binds the matrix and fiber [15,16].

There is frequently no filler metal and no liquid fusion in diffusion bonding. The joint typically displays the strength and temperature resistance of the base metal(s) with no additional weight added. There is extremely little to no plastic deformation of the materials. There is no bonding process contamination and very little residual stress is created. In theory, it can be applied to any size joint surface with no increase in processing time; in practice, though, the surface is usually constrained by the necessary pressure and physical constraints. Pieces of different thicknesses, reactive and refractory metals, and comparable and dissimilar metals can all be used for diffusion bonding.

Pressure and heat are applied to the components during diffusion bonding, often for many hours (Figure 6). The surfaces are heated using electrical resistance or in a furnace. A hydraulic press can be used to apply pressure at a specific temperature; this technique enables precise load measurements on the components. Differential thermal expansion can be utilized to impart load in situations where there cannot be any temperature gradient among the pieces. When low-expansion metals, like molybdenum, are used to fix parts, the parts will supply their own load since they will expand more with temperature than the fixture metal. Other techniques for exerting pressure are high-pressure autoclaves, differential gas pressure between the two surfaces, and the use of dead weights. When working with metals that have thick oxide layers, such as copper, diffusion bonding needs to be carried out in a vacuum or inert gas atmosphere. Diffusion pressure, temperature, and surface treatments, including cleaning, etching, and polishing, are crucial elements in the diffusion bonding process.

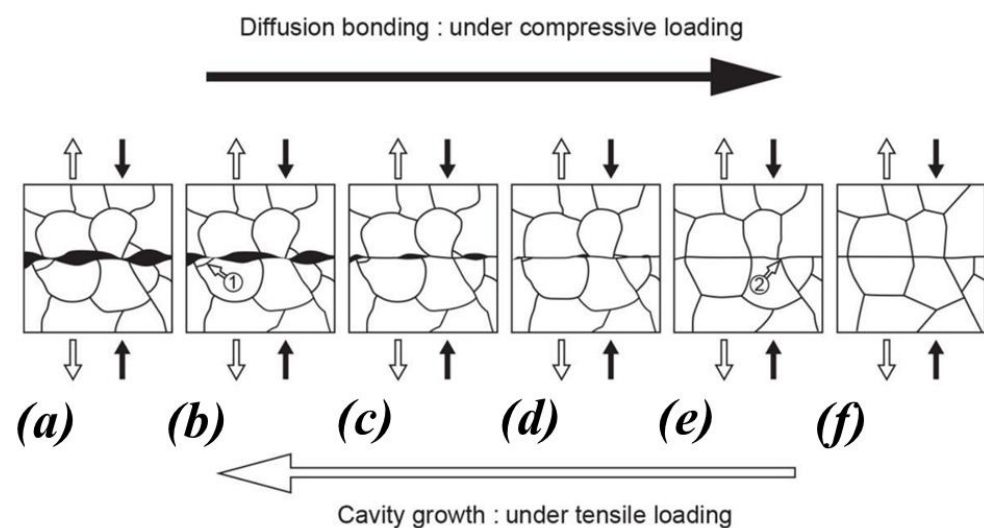


Figure 6. Mechanism of the solid-state diffusion bonding: (a) surface contact, (b) onset of diffusion bonding, (c) evacuation of gases from the voids, (d) voids shrinkage, (e) voids elimination, and (f) formation of a voids-free interface [17].

Diffusion bonding has been utilized in earlier research to develop SiC particle-reinforced AMCs (Al/SiC_p-MMCs) [18]. In this series, Zhang et al. observed that obtaining adequate bonding quality in the diffusion-bonded Al/SiC_p-MMCs is more challenging and that the strength of vacuum diffusion-bonded components diminishes with an increase in SiC_p contents. When it comes to diffusion bonding, whether it is for similar or dissimilar Al/SiC_p-MMCs, the application of an appropriate insert alloy layer can clearly enhance the joint strength. Additionally, the strength of diffusion joints that use an insert alloy layer appears to be higher than that of joints that do not use one.

The SEM scans (Figure 7a) show many reinforcer SiC_p particles in the joint specimen's joining interface. These particles resembled inclusions, which often have weak bonds with the matrix of aluminum alloys. It appears that a higher proportion of SiC_p in the volume results in more SiC_p reinforcers in the joint joining interface. This, in turn, leads to further weakening micro-joining interfaces in the joint interface region and, ultimately,

reduced joint strength. Since there are numerous SiC_p reinforcers in the joint's interface, the diffusion-bonded joint shown in Figure 7b has a higher SiC_p volume percentage of 20%, which results in a very low joint shear strength.

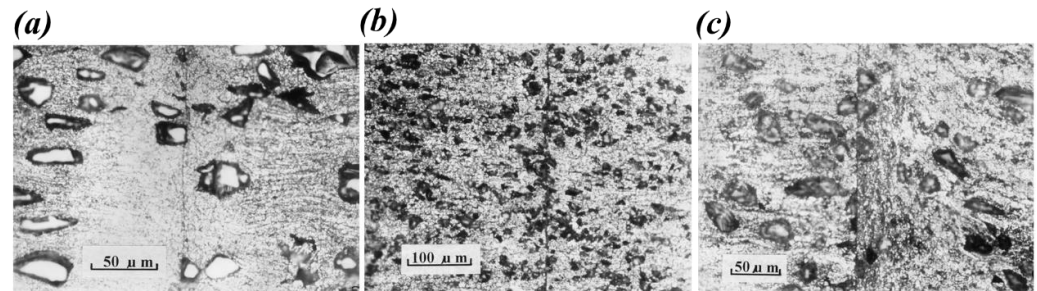


Figure 7. Microstructure of diffusion bonded joints (a) 10% SiC_p /2024Al (b) 20% SiC_p /6061Al (c) 5% SiC_p /2024Al, right: 10% SiC_p /6061Al [18].

When it comes to metallic materials, it is generally far easier to link comparable materials together than dissimilar ones. The vacuum diffusion bonding of Al/ SiC_p MMCs leads to the same result as well. It appears that as the SiC_p volume percentage increases during vacuum diffusion bonding of different composites, the joint strength correspondingly decreases. Diffusion-bonded joints having a greater SiC_p volume percentage might be almost as strong as joints with a lower SiC_p volume percentage if the right insert alloy layer is utilized.

3.1.3. Friction Stir Processing

A technique called friction stir processing (FSP) uses strong, focused plastic deformation to alter a metal's characteristics. The process that causes this deformation involves pushing a non-consumable tool laterally through the workpiece while rotating it in a stirring action. In its most basic form, FSP is just a non-consumable rotating tool that is inserted into a work component and rotated in the desired direction. Figure 8 displays the schematic illustration of the FSP. The tool's two main purposes are to heat the workpiece and deform the material of the workpiece. Heat is generated mostly by friction between the spinning shoulder and the workpiece, although the revolving pin also stirs the heated material.

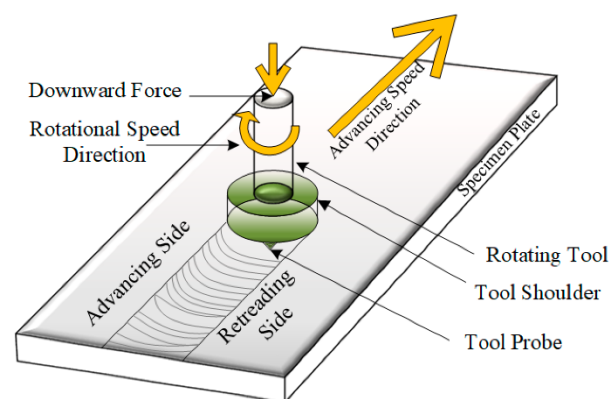


Figure 8. Schematic of an FSP process [19].

The heated substance stirs across the revolving pin and softens; then, the tool's back void is filled up [20]. Significant microstructure refinement occurs in the treated zone as a result of the material curving across the tool being exposed to extreme heat and plastic deformation. The zone stirred by the tool pin is named as stir zone (SZ). The primary mechanism responsible for producing refined and equiaxed grains in the SZ is dynamic recrystallization (DRX). But in materials with significant stacking fault energy, like Al alloys, dynamic recovery happens before DRX [21].

The ability of FSP to fabricate surface composites in all their variations with minimal or no interfacial reactivity to the reinforcement has been observed. Surface composites were created in the past by layering ceramic particles in a volatile liquid. Currently, the grooved workpiece serves as a reinforcement house for the ceramic particles. The main methods for fabricating surface composites using FSP are schematically given in Figures 9 and 10.

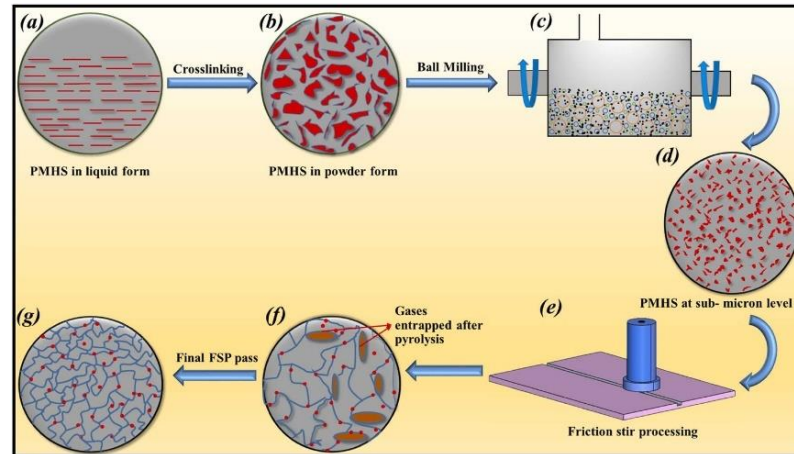


Figure 9. The steps taken to create PMHS polymer: (a) as-received liquid PMHS; (b) PMHS polymer in solid state following an 8 h cross-linking process using 5 weight percent DABCO; (c) employing a ball mill method that was developed domestically to grind solid PMHS polymer into a fine powder (d) PMHS polymer that has been ball milled and has submicron particle size (e) and filling Al matrix with FSP of submicron polymer particles. (f) Polymer particle dispersion in Al matrix (revealed by red dots) and (g) gas inclusion resulting from the ceramic composite's 10 h pyrolysis at 500 °C ceramic matrix created from polymers following the final FSP, following the extraction of all trapped gasses and the fine dispersion of ceramic particles using Al matrix [4].

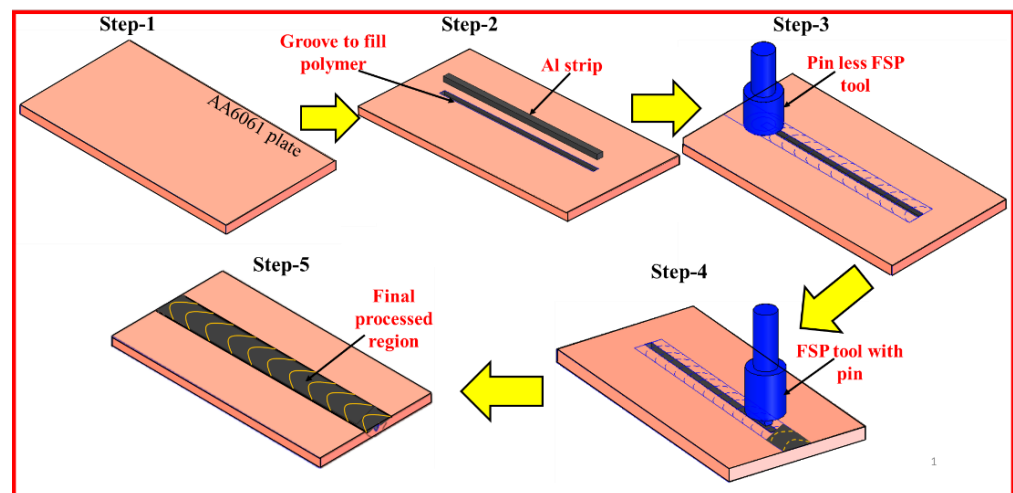


Figure 10. Schematic showing the processes taken to develop the PDC-MMCs of AA6061. (Step 1) From bulk metal sheet, an AA6061 plate with the necessary dimensions is cut along the rolling direction. (Step 2) At the center plate region, a groove of 3 mm in depth, 4 mm in width, and 150 mm in length is formed. To conceal the groove, a strip the same size and material as the groove is likewise cut. (Step 3) The groove is filled with ball-milled PMHS and sealed with an aluminum strip. Moving down the groove line, a pinless FSP tool is used to pack the polymer inside the matrix. (Step 4) mixing and scattering of polymer in Al matrix is carried out via FSP. (Phase-5) [4].

While experimenting with AMCs based on PDC, as in Kumar et al. [4], Figure 11 shows the 3D topographies of wear regions under various loads of polymer-derived

composite (PDC) developed using polymethylhydrosiloxane (PMHS). To fully understand the results, line graphs showing wear depths in longitudinal and transverse directions were complemented with 2D morphology. While the wear track of BM was wavy and erratic, that of AMCs was smooth and nearly symmetrical for the majority of the cases under study. This suggests that compared to BM, AMCs may provide better resistance to wear at greater typical loads. It is evident that the samples lacking ceramic nanoparticles have deeper surface grooves than the samples that include them (Figure 11). This results from the AMCs' (240 HV0.1) and base metal's (50 HV0.1) significantly different hardness levels. The HCHC pin has the ability to pierce non-reinforced metal surfaces, forming a deep puncture that results in significant material loss and severe plastic deformation. In contrast, uniformly distributed particles on the surface serve as barricades for dislocation movement, and so attempt to lessen plastic deformation [22]. High hardness stops wear on the composite surface and the pin from penetrating deeply.

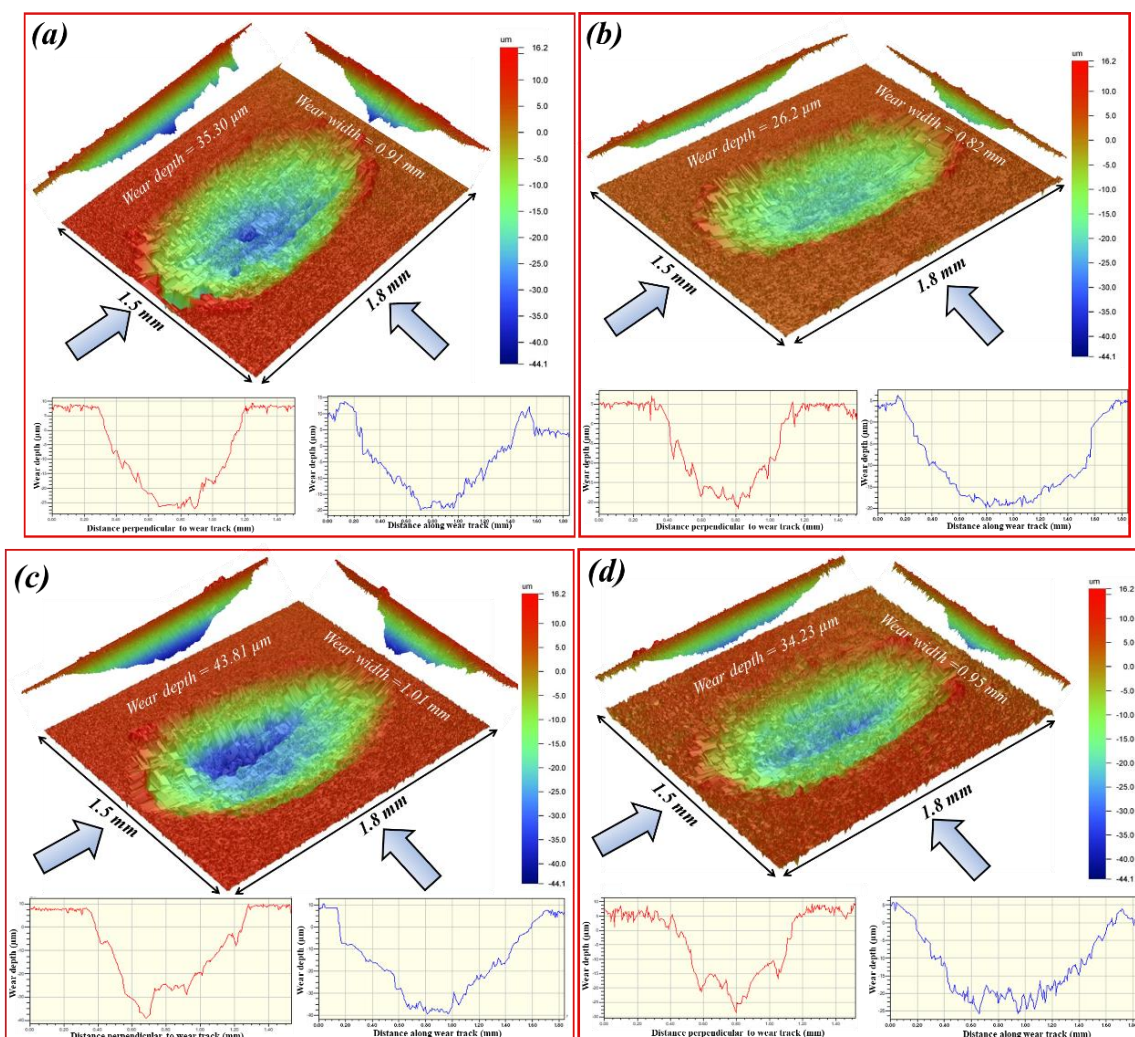


Figure 11. Profilometer data of wear track. Three- and two-dimensional topography, line diagram for wear depths along and perpendicular to the wear track (a), and (c) for BM at 1471.0 and 1961.3 mN loads and (b) and (d) for polymer composite at 1471.0 and 1961.3 mN loads, respectively [4].

Intermetallics are brittle in nature and provide the soft edge to initiate and propagate the cracks in the weld/processed region of dissimilar metal interfaces. Though their formation is unavoidable, a few techniques have been developed to suppress them [23–25]. Akramifard et al. [26] developed SiC/Cu surface composites using the FSP process. They obtained an even dispersion of reinforcements with reduced agglomerates in the metal

matrix. The microhardness of MMCs was two times higher than substrates, while SiC could have improved wear properties. This study could not notice any intermetallic formation. Lim et al. [27] developed AA7075 MMCs using multi-walled carbon nanotubes (MWCNTs) via FSP and suggested that multi-passes might enhance the nanotube distribution. As per their suggestion, higher tool rotation and higher plunge depth might improve the homogeneity of nanotubes in the MMCs. However, an entirely even dispersion was not attainable once the regularly tangled nanotubes were added. Toth et al. analyzed high-temperature grain stability while adding polymer-derived composites in the Al metal matrix. They noticed steady grain structure having a minor reduction in hardness even after exposing the MMCs to high temperatures for considerable duration (450 °C and 550 °C for 1 h). It may be attributable to particle pinning of grain boundaries due to the Zener mechanism. To fabricate polymer-based MMCs, Azarsa et al. [28] incorporated high-density polyethylene (HDPE) and copper powder as matrix and additive metal powder, respectively. They obtained uniform intermixing of metal particles with polyethylene. Consequently, MMCs with excellent ultimate tensile strength and ductility are obtained. Kumar et al. [29] noted a uniform distribution of nano-sized polymer-derived silicon carbonitride (SiCN) in the matrix. The MMCs obtained had high microhardness, nearly five times that of the base metal. Negligible tool wear was reported by this route due to the in situ soft dispersion of polymer particles. Cao et al. [30] developed in situ C-fiber-Al composites by using in situ FSP method. In MMCs, massive intermixing of carbon fibers with the metal matrix was foreseen without any prominent layer of Al₄C₃. The hardness, strength, and elongation of the MMCs were enhanced significantly more than the base metal.

3.2. Additive Based Techniques

3.2.1. Physical Vapor Deposition

The phrase “physical vapor deposition” (PVD), often referred to as “physical vapor transfer” (PVT), refers to a group of vacuum deposition methods that may be utilized to form thin films and coatings on substrates made of metal, glass, ceramic, and polymers. During the PVD process, the material transits from a condensed phase to a vapor state and back to a thin film condensed one. The two preferred PVD methods are sputtering and evaporation. PVD is widely adopted for manufacturing goods that necessitate thin coatings for mechanical, electrical, optical, or acoustic functions, among others. Such as semiconductors and thin-film solar cells [28], aluminized PET film for food packaging and balloons, microelectromechanical devices such as thin-film bulk acoustic resonators, and titanium nitride-coated cutting tools for metalworking. A power supply unit provides thermal energy to raise a liquid or solid source’s atoms’ temperature up to its evaporation. After traveling a path (sometimes in a vacuum chamber), evaporated atoms settle upon the heated substrate. After a continuous evaporation procedure, a thin film is created. The power supply unit could be a pulsed laser, heating wire, electron beam, molecule beam, etc., depending on the approach used. It should be noted that certain evaporation deposition techniques, such as activated reactive evaporation, also involve chemical reactions between the deposition sources. A modern PVD system’s essential parts have been displayed in Figure 12. Activated reactive evaporation is typically used to deposit ferroelectric thin films, where reactions between sources and oxygen gas occur on the substrate. For instance, a thin film can be created for a standard perovskite ferroelectric, ABO₃, by evaporating the sources of A and B so that they can react with the oxygen gas that is supplied [31]. The reaction equation involved may be:



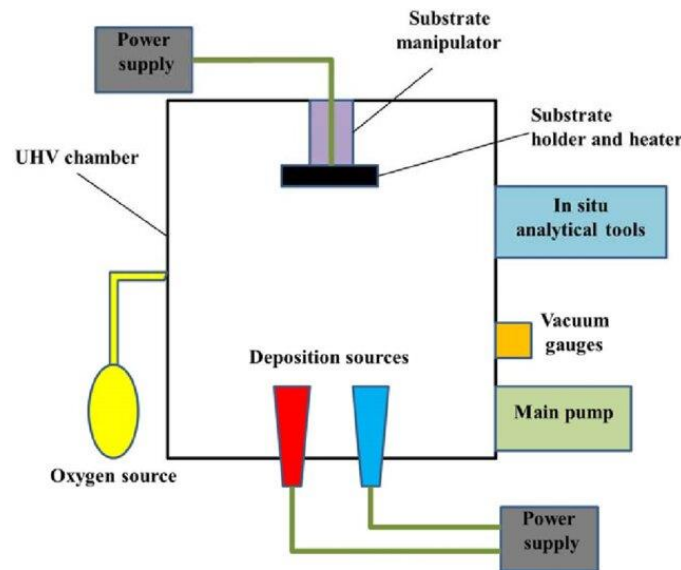


Figure 12. Schematic of a typical physical vapor deposition process [32,33].

When it comes to the environment, PVD is more costly than traditional coating processes. As previously noted, electrodeposition uses a number of hazardous solutions; as a result, a large amount of water is needed to comply with environmental requirements. However, the high temperature (460–700 °C) that the HDG process needs for the substrate results in a significant energy requirement and an ecological footprint. This technique's environmentally friendly steps—evaporation, transit, reaction, and deposition—are what make it appealing. In contrast to wet chemical processes, the PVD process does not require the disposal of chemical waste that poses a major threat to the environment. Furthermore, no wastewater, toxic gas, or other residue is released during the PVD process. The PVD process's ability to deposit material at low substrate temperatures—up to 250 °C is adequate—means no probability of brittle intermetallic compound formation at the dissimilar interface, which would weaken the interlayer bonding strength. Furthermore, as the complete deposition process occurs in a vacuum, the production of oxide layers on steel sheets—a common worry in the HDG process—never has the chance to impede adhesion. These benefits maintain the PVD process a few steps ahead of the traditional methods employed by steel firms.

3.2.2. Selective Laser Melting

Particularly adaptable for processing a range of powder materials for composite manufacture is selective laser melting (SLM). Because new ingredients are generated in laser melting, this adaptability permits the dispensation of reactive primary powder material systems, i.e., obtaining different materials than the beginning powder combinations. In SLM, a metal-based powder bed is selectively fused layer by layer with a laser to create a set of specified cross-sections [34] (Figure 13). In the case of MMCs, the laser is not only utilized in fusing powder particles; if the powder combinations have the capacity to react chemically, they can also start a reaction. Due to its layer-by-layer, laser-based, and simultaneous powder metallurgy processes, SLM is able to produce composites from any desired mixture—even reactive materials—with consistent secondary phase dispersion in geometrically complex structures with remarkable flexibility.

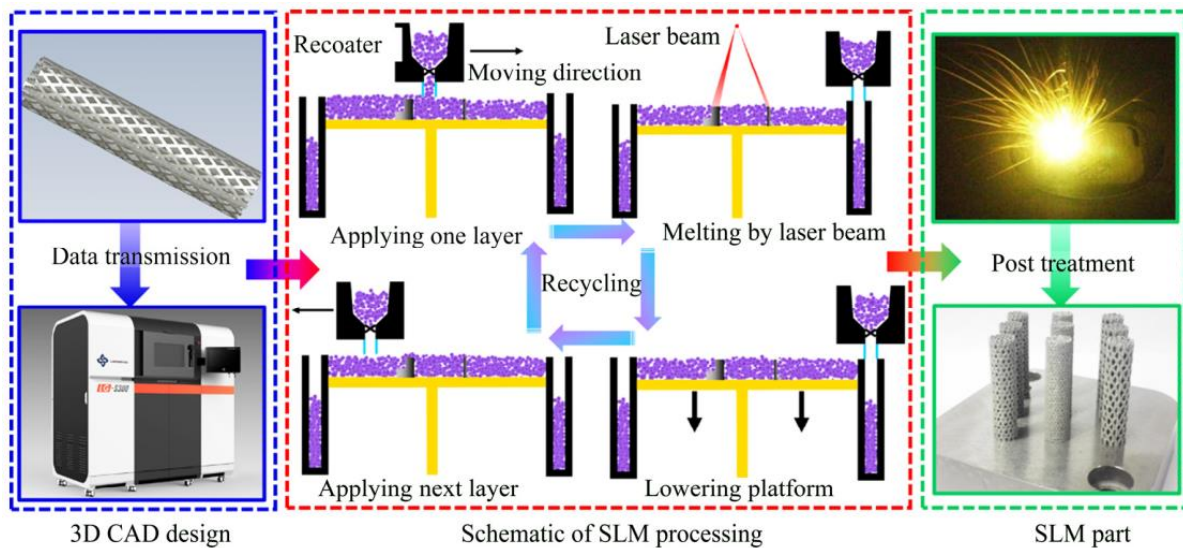


Figure 13. Typical stages in SLM production [35].

Because of the laser beam's high scanning speed, SLM causes the powder material to be exposed to a heat source for a considerable time, which causes rapid heating and melting followed by quick solidification. The melt pool's size and geometry, the pace of cooling, and chemical reactions across the melt pool and heat-affected zone are all influenced by the resulting heat transfer, fluid movement (such as Marangoni flow), and the existence of secondary phases. Porosity, balling, residual strains, cracks, and hot ripping are some of the typical quality problems that might arise during SLM [36].

Al MMCs have mostly been examined by reinforcing with TiC [37,38] Al_2O_3 , [37] carbon nanotubes, [37] SiC, or Mg_2AlO_4 . The additional reinforcements should normally be extremely fine in the nano-size range in order to positively impact mechanical performance. Since Marangoni convection is weakened by SLM at a low laser energy of 250 J/m , solid TiC particles may descend to the ground and clump together as a result of gravity [34]. Therefore, to achieve a consistent spread of reinforcements, raising laser intensity may enhance the flow and dispersion of TiC reinforcements. On the other hand, too strong a laser beam could pulverize the particles and damage their mechanical and microstructure [35,37]. Due to these challenges, the microstructure of "ex situ" composites is frequently reported to be highly diverse and non-uniform; for instance, a non-homogeneous spreading of secondary phases in laser-processed Al-7Si-0.3Mg-10%SiC may be seen in Figure 14.

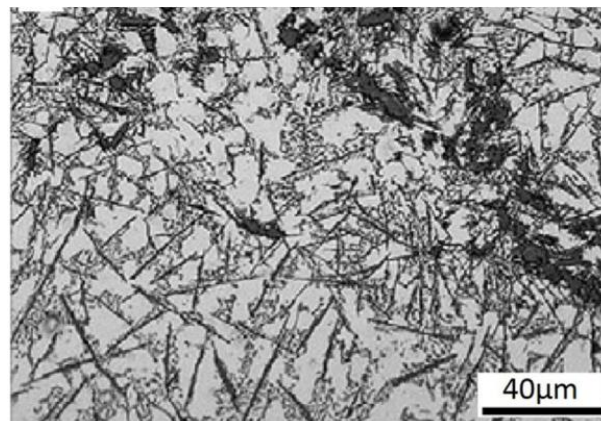


Figure 14. A thickness-based optical micrograph displaying the microstructure of specimens sintered using a laser from an Al-7Si-0.3Mg-10% SiC powder mixture [34,39].

The thermodynamics of the Al_2O_3 phase at elevated temperatures can cause diffusion and the reaction of Al_2O_3 in the Al matrix, which may result in the production of pores. With improved settings, irregular flaws are detected surrounding the Al_2O_3 phase, as Figure 15a illustrates. Liao et al. [40] examined the equilibrium stages of non-standard state reaction between Al and Al_2O_3 throughout the SLM process. According to their findings, the primary mechanism for Al_2O_3 loss is the reduction reaction between Al_2O_3 and Al. This reaction is necessary for Al_2O_3 loss since the melt pool's temperature is higher compared to the reduction reaction's critical temperature (1793 K). Al_2O_3 might not directly evaporate in the SLM process, as Figure 15b illustrates, and the development of Al_2O gas may alter the thermophysical actions of the Al matrix in the melt pool [40]. Consequently, careful consideration should be given to reinforcement in the case of SLM Al matrix composites and the advancement of forming principles should be prioritized over simple parameter optimization for fabricating nearly fully dense Al matrix composites without defects.

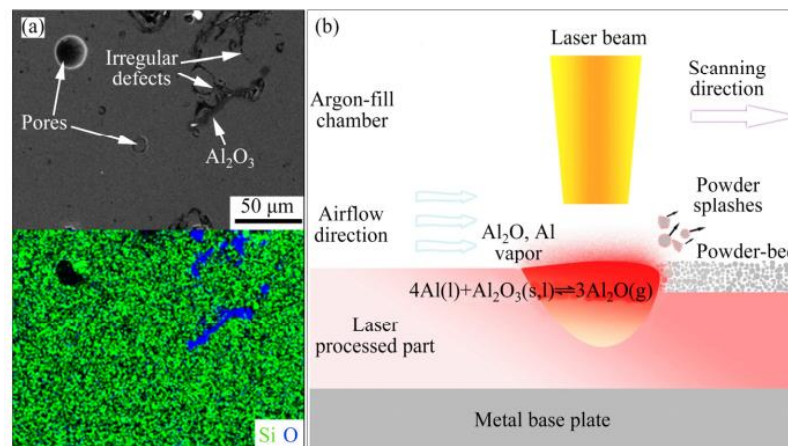


Figure 15. SEM EDS of $\text{Al}_2\text{O}_3/\text{Al-12Si}$ composites printed using SLM (a), and schematic of Al_2O_3 loss (b) [35,40].

3.2.3. Direct Energy Deposition

Using a concentrated energy source, such as a laser, plasma arc, or electron beam, Directed Energy Deposition (DED) or Laser Deposited Additive Manufacturing (LD-AM) is a 3D printing technology that melts material simultaneously with nozzle deposition. As with other additive manufacturing methods, DED systems can be used to add material to components that already exist, for repairs, or infrequently, to manufacture new parts. The DED process is also known as Direct Metal Deposition (DMD), Laser Engineered Net Shaping (LENS), Electron Beam Additive Manufacturing (EBAM), Directed Light Fabrication, and 3D Laser Cladding, depending on the specific application or technique used [41]. Figure 16 displays the LD-AM process schematic diagram. Initially, heat from the laser beam selectively melts the substrate, creating a molten pool that collects and melts powders from a powder stream. The molten pool begins to harden due to heat dissipation when the laser beam goes away. Forming the first layer on the substrate, the deposition head follows the predetermined path using a 3D file. The deposition head then travels up one layer thickness to a newly defined point in preparation for the corresponding layer deposition. The first layer, which was acting as the new “substrate”, partially melts as the second layer forms. Until the intended near-net form component is constructed in subsequent layers, similar procedures will be carried out numerous times.

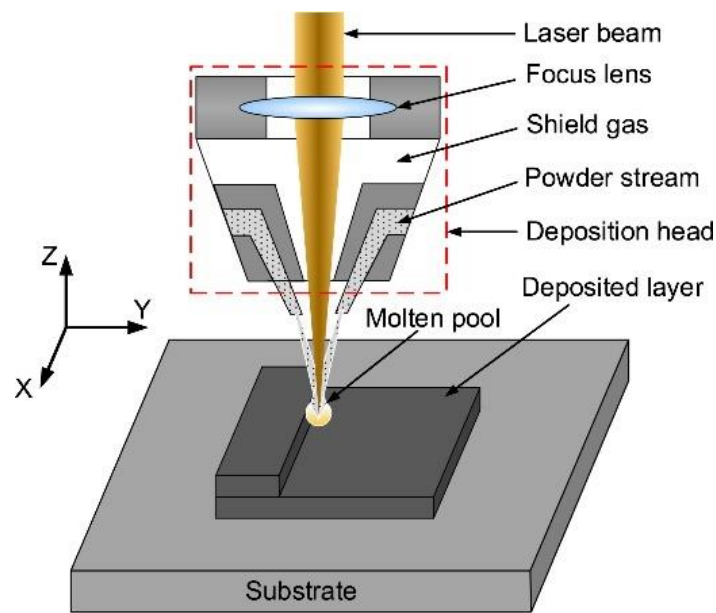


Figure 16. Schematic of LD-AM process [42].

Balla et al. used the LD-AM procedure to successfully create dense and net-shaped Al_2O_3 deposits (cylinders, cubes, gears, etc.) [43]. According to experimental data, columnar grains developed along the direction of construction, and the mechanical properties of the manufactured components were anisotropic. The effects of laser power, scanning speed, and powder feeding rate on printing attributes (dimensions, surface roughness, flatness, powder efficiency, and microhardness) in LD-AM of Al_2O_3 were investigated by Li et al. [44]. Wu et al. observed that in addition to deposition quality, varying LD-AM process parameters led to variations in the hues (white/black) of the manufactured Al_2O_3 thin-wall structures [45]. The creation and spread of interior defects, as well as an increase in the amount of entrapped gas, shrinkage discrepancies, and oxide impurity volatility, would occur from the emergence of these second phases which are black in color. Additionally, the investigators discovered that the surfaces of the black construction displayed densely spaced fissures that expanded in the direction of the build. The white structure had far fewer cracks than the black structure, most of which were on the upper surface. Optimizing the LD-AM process parameters is important if desired part quality and attributes are to be achieved. A mathematical model that might show that a connection between process factors and physical characteristics of manufactured Al_2O_3 components was created in order to save arduous tests for determining the ideal process parameters [46]. Niu et al. used pure ZrO_2 and Al_2O_3 powders with a eutectic ratio of 41.5 weight percent to 58.5 weight percent to successfully develop cylindrical and arc-shaped ZrO_2 - Al_2O_3 eutectic microstructures via the LD-AM process [47]. As illustrated in Figure 17, a fine-grained microstructure with a eutectic spacing of 100 nm was created as a result of the LD-AM's quick melting and solidification process. It has been stated that the LD-AM process was improved and homogenized by adding ultrasonic vibration [48]. Components manufactured by LD-AM added with ultrasonic vibration demonstrated better mechanical characteristics than components made without ultrasonic vibration. Hu and colleagues manufactured ZrO_2 - Al_2O_3 bulk parts having a weight ratio of 10 weight percent: 90 weight percent between ZrO_2 and Al_2O_3 using the ultrasonic vibration-assisted LD-AM technique [49]. An analysis of the impacts of acoustic addition revealed improved microhardness, wear resistance, and compressive properties while also reducing grain size.

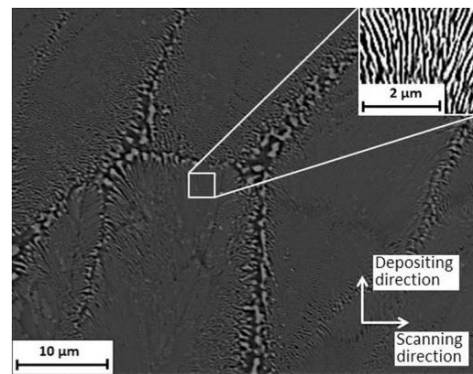


Figure 17. Eutectic microstructure of an LD-AM-fabricated $\text{ZrO}_2\text{-Al}_2\text{O}_3$ [42,47].

3.2.4. Cold Spraying

The application of the CS process as a coating technology has been widespread across numerous manufacturing units, such as automotive, marine, medical, energy, and aerospace. Deposits of the CS layer offer highly efficient defense against extreme heat, oxidation, erosion, corrosion, and other chemical reactions [50–52]. The CS technique has been implemented as an AM technology [53] in the last few years to create solid metal 3D builds and repair cracks [54,55]. Given that CSAM offers most of the benefits of the cold spray approach, this motivated the expansion of the research in deeper domains. Compared to traditional fusion-based AM processes, CSAM offers a number of benefits, including reduced production times, low input temperatures, significant plastic deformation across the interfaces, smaller part sizes, increased flexibility, and the capacity to fix broken components [56].

The particles' kinetic energy, or the supersonic impact of particles, is the primary basis of the CSAM process mechanism. The hot gas propels powder particles that are transported by a cold, compressive gas, at a temperature of 25 °C to 1000 °C at a supersonic velocity. Upon impact on the surface, the kinetic energy of the particle is transformed into plastic deformation. Particles impacting at supersonic speeds create bonds that cause the oxide layers at the surface to completely shatter, which causes the material to jettison (Figure 18) [56–58]. Additionally, it has been noted that bonding occurs when the surface craters and particles mechanically connect upon impact.

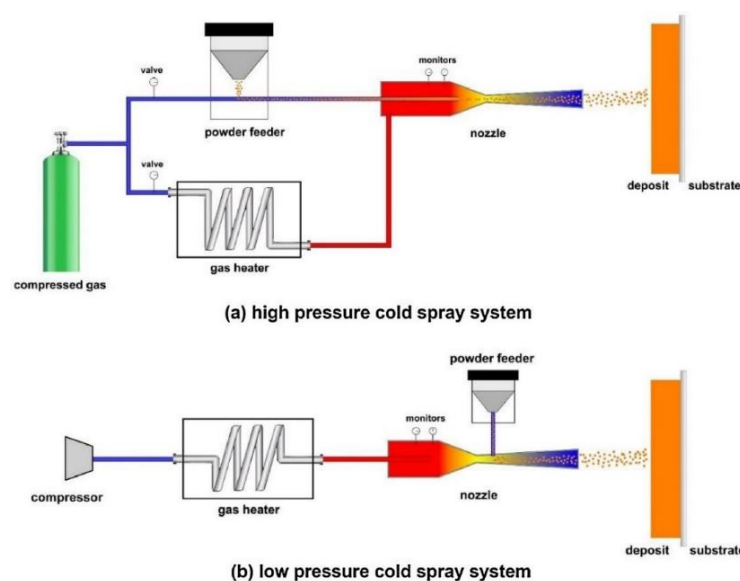


Figure 18. (a,b) Schematic of high-pressure and low-pressure cold spray techniques [56].

Even though the CS technique was primarily created for metal coating in the early 1980s, this has now evolved into a substantial and cutting-edge AM technology in recent decades [56]. The ideal gas parameters are used by powder particles driven by hot gases like helium (He), nitrogen (N₂), and air. Very high particle velocities are the result of the gas's increased temperature, pressure, and molecular weight [59]. Despite its high cost, helium offers stronger bond formation and increased deposition efficiency. This enhances the build component's ductility and density, and it does so in a better manner than nitrogen produces [58,60,61]. Nitrogen gas results in poor mechanical characteristics; to lessen the brittleness of Cu deposits sprayed with nitrogen, post-processing steps like annealing are required [62]. It is discovered that some parameters, such as spray angle and gas temperature, are directly and linearly correlated with deposit density and strength [63]. The build quality is also influenced by parameters including the scanning step, nozzle trajectory, standoff distance, nozzle traverse speed, and powder feed rate [56]. Higher oxygen concentration powders are found to have a worse deposition efficiency [59].

Researchers and industry have shown interest in AMCs made using CSAM thus far because of its enormous potential and suitable qualities for application in aircraft and maritime. Previous reports state that the precise and appropriate addition of ceramic reinforcement with Al matrix may enhance the mechanical performance of CS Al metallic composites, including microhardness and wear performance [64–67]. However, because of inadequate bonding across ceramic particles Al interface, it is difficult to achieve good tensile characteristics [68]. According to Kumar et al. [69], low tensile strength and poor ductility caused CS SiC/Al composites to fracture even in the early phases. Examining the fracture surface indicated that the SiC/Al matrix and inter-splat contacts were not well bound, which led to the formation of a brittle fracture.

Xie et al. [70] suggested using a novel hybrid gas-atomization method that included post-FSP, CS, and in situ reactions to create a nano-TiB₂/AlSi₁₀Mg composite. The electron backscatter diffraction (EBSD) maps of the homogenous structure with equiaxed, fine grains are displayed in Figure 19. The FSP specimen has a homogenous structure because of its dynamic and continual recrystallization. Constant inclusion of the strain is combined with quick recovery and sub-grain/border movement [71].

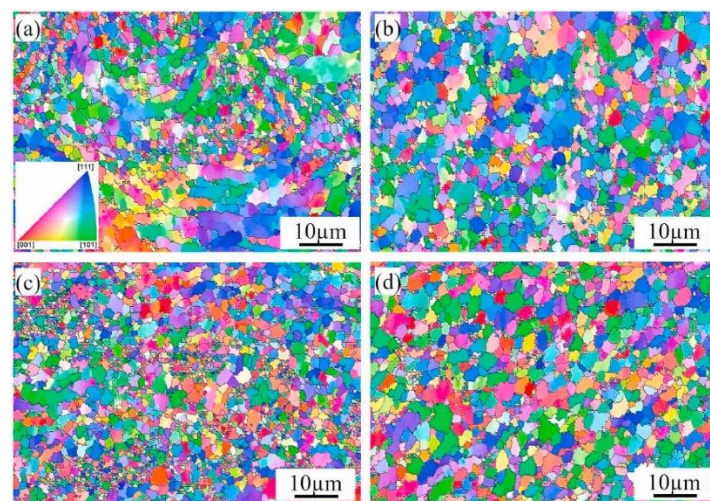


Figure 19. SEM/EBSD maps of the (a,b) CS and (c,d) CS + FSP samples in high magnification: (a,c) AlSi₁₀Mg; (b,d) TiB₂/AlSi₁₀Mg composite [70].

In FSP, there is significant plastic deformation in and surrounding SZ. As a result, there are many dislocations and their corresponding interaction movements. Dense dislocations caused by stored energy result in dynamic recovery and recrystallization. TiB₂ nanoparticles are primarily responsible for the composite sample's refinement since they obstruct dislocation motion followed by recovery. CS deposits using gas-atomized AA 6061

powder were attempted by Wang et al. [58]. The main focus of the experiment is to examine how spray angle affects bonding strength and how it relates to deposition efficiency and component strength. Figure 20 displays, for impact velocities, temperature contours on the deformed objects. Particle penetration increases and its flattening improves with a rise in impact velocity. This signals the formation of a stronger, faster-forming mechanical interlocking link. The cause of the elevated temperature is due to adiabatic heating, a phenomenon that is often observed at a higher impact velocity. Additionally, at a maximum impact velocity of 980 m/s, localized melting is seen. These trends also suggest that sound metallurgical bond formation would occur at higher impact velocities.

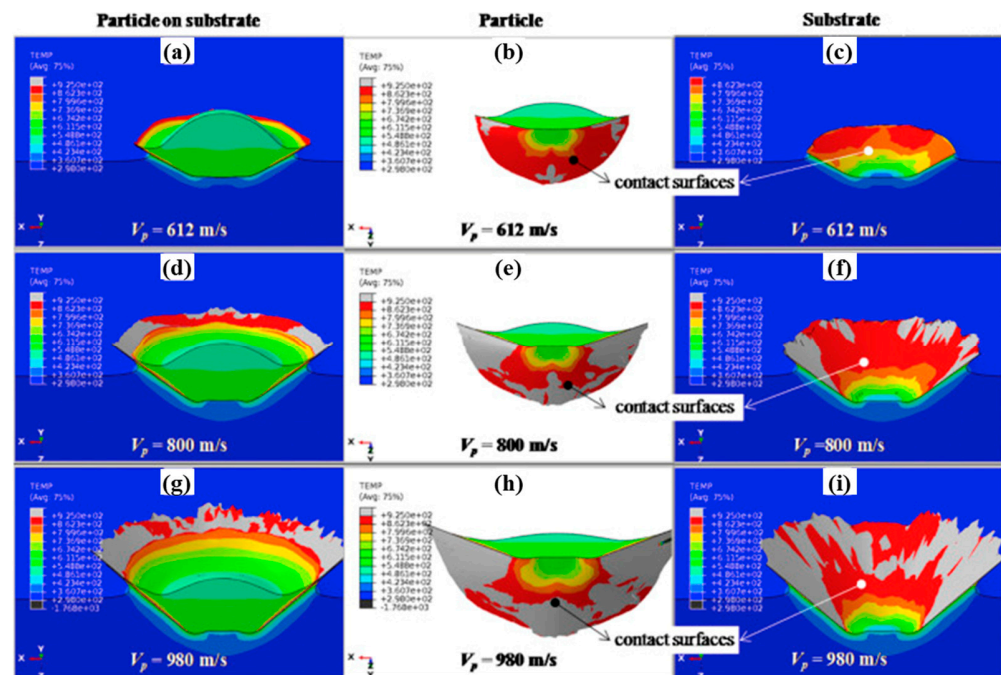


Figure 20. Temperature plots of the deformed particle and substrate at the impact velocities of (a–c) 612 m/s, (d–f) 800 m/s, and (g–i) 980 m/s [58].

3.3. Liquid-State-Based Techniques

3.3.1. Stir Castings

Stir casting is one of the most affordable approaches for developing huge near-net form parts from MMCs [72] and is frequently utilized in the commercial sector. Also known as the vortex technique, this method was created by using powder metallurgy to reinforce particle fillers into an aluminum metal matrix. Making a melt of chosen matrix material, adding a reinforcing material, and stirring melt to obtain the right dispersion are typical steps in the stir casting process. The rotating impeller uses the vortex process to create a molten alloy vortex, to which pre-treated ceramic particles are added. During the stir-casting process, reinforcements are added to a liquid aluminum melt and the mixture is allowed to harden. Achieving sufficient wetting in this instance is critical between particle reinforcement and liquid melting of the Al alloy. The qualities of composites made with this method can be altered by adjusting a number of process variables, such as the size and placement of the stirrer and the temperature at which the composite is poured, heated, processed, melted, and retained [73,74]. To achieve a homogenized mixture of reinforced particles in the metal matrix, a number of manufacturing parameters must be controlled, including crucible size, impeller ability and size, temperature of the molten metal, stirring time, stirring speed, rate of particle feeding into the mixture, and mold temperature [75,76]. Two main issues with this procedure are that, first, the liquid metal matrix does not usually moisten the ceramic particles, and second, the dispersion of ceramic elements can be

irregular since the reinforcing particles have a tendency to sink or float based on their density in conjunction to molten metal [16].

3.3.2. Infiltration Process

When powder compact is submerged in melted metal or comes into contact with it, liquid metal fills the holes in the compact due to surface energy, creating materials with a high relative density. This process is known as the infiltration method. Capillary forces play a role in the mechanism by which the molten metal fills the pores during penetration. The depth and rate of infiltration can be evaluated as [77,78]:

$$\text{Infiltration depth} = \frac{2\tau \cos \theta}{\rho g r} \quad (1)$$

$$\text{Infiltration speed} = \frac{r\tau \cos \theta}{\pi \mu} t \quad (2)$$

where τ is the liquid–air surface tension, θ is the angle of contact, ρ is the density of metal in a molten state, r is the radius of the capillary tube, t is the infiltration time and μ is the viscosity of the molten metal.

To create gradient MMCs by infiltration, a porous preform having gradient pore circulation must be prepared. Next, liquid metal must be infused into the preform, and lastly the infused preform must be chilled to an ambient state. The magnitude of pressure required to intermix reinforcement and matrix relies on how much of the molten matrix fills the ceramic preform and causes friction due to its viscosity. Numerous variables, including alloy composition, material and surface shape of the ceramic preform, temperature, and time, affect how liquid alloy wets the ceramic preform [79]. Pressure or vacuum can be applied to the preform to facilitate infiltration, based on the type of reinforcement and its quantity utilized. There are numerous ways to generate AMC with reinforcement volume fractions between 10 and 70% through infiltration procedures. It is frequently required to have silica and alumina as a binder to maintain its integrity and shape. In the infiltration technique, porosity and regional modifications in volume percentages in AMCs are commonly encountered. The method is normally employed in developing AMCs reinforced with particles, whiskers, short fibers, porous skeletons or continuous fibers [6].

3.3.3. Spontaneous Infiltration Process

There is no application of outside pressure or force during a spontaneous infiltration process. Because the pressureless infiltration approach makes it possible to create materials with large ceramic percentages without the need for an external force, it is a desirable method for producing metal–ceramic composites. The molten metal should moisten ceramic for spontaneous infiltration to happen, and there must be less than a 90° contact angle between the surfaces of the two materials. In order to drive metal into the porous preform, it encourages capillary phenomenon. However, no infiltrations into the porous material will happen when the contact angle is larger than 90° because the molten metal may not moisten the ceramic substance. Put another way, spontaneous infiltration happens when the reinforcement and matrix have good wettability. The reinforcement may, however, be coated with an element or compound to increase the wettability and, consequently, the infiltration of the liquid metal into the ceramic matrix, if there is insufficient wettability between the reinforcement and matrix [80]. The brief outlines of the pressureless infiltration process are shown in Figure 21.

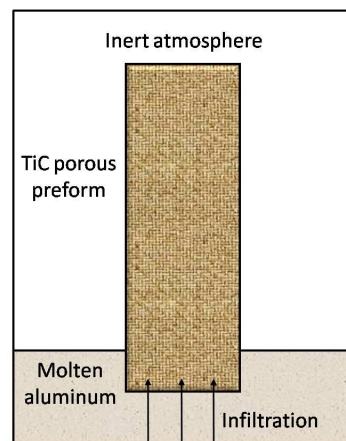


Figure 21. Pressureless infiltration process for the Al/TiC system.

Due to its low density and good thermal conductivity, Al alloys are a promising material for the majority of metal–ceramic composites. Its high thermal expansion coefficient and poor strength are drawbacks, though. Its mechanical characteristics and resilience to high temperatures are both enhanced by adding TiC or SiC. The amount of ceramic material and the manufacturing parameters influence the mechanical qualities of composites that are created. However, due to the high volume percentage of reinforcements, these composites have good mechanical and physical properties [80].

The technique of pressureless infiltration into SiC preforms has been extensively studied utilizing alloys like Al-Si, Al-Mg, and Al-Zn. However, numerous obstacles remain, restricting the application of this approach in industrial settings. The development of a strong bond between reinforcement and matrix necessitates a high degree of wettability between the two. However, during the liquid state manufacturing process, when the alloy interferes with reinforcement, interfacial reactions may occur. These reactions can result in brittle products, based on temperature, composition and interaction time. The main disadvantage of pressureless infiltration, which results in the formation of oxide layers across melting regions, is poor wettability between reinforcement and matrix. In Al-SiC-based composites, poor wettability causes unfavorable reactions at the interfaces and slows down the manufacturing process, which, in turn, causes the development of intermetallics such as Al_3SiC_4 and Al_4C_3 [16].

Recently Amosov et al. [81] proposed a new method to manufacture the metal/ceramic composites of IPCs type, including Al/TiC, using the process of Self-propagating High-temperature Synthesis (SHS) of a porous ceramic skeleton formed during the combustion of mixtures of initial powder reagents, followed by spontaneous infiltration by metal melt. Since the wetting of ceramic phases with aluminum melt significantly improves with a temperature increase of more than $1000\text{ }^\circ\text{C}$, the very high temperature (more than $2000\text{ }^\circ\text{C}$) of the synthesized ceramic skeleton provides very good wettability and very fast (within a few seconds) complete spontaneous infiltration of such a skeleton with an adjacent aluminum melt, followed by rapid cooling of the formed composite without the formation of undesirable intermetallic and carbide phases of aluminum.

3.3.4. Forced Infiltration

In this melt, the metal is pushed into the porous reinforcement using the forced infiltration process, which is controlled by mechanical force or external pressure. By applying mechanical force to press the liquefied metal into a preform, it avoids the problem of insufficient bonding between reinforcement and matrix. A variety of forced infiltration is available, as discussed hereafter.

Pressure Die Infiltration Process

This is a mechanical infiltration technology that was modified from the unreinforced metal die-casting process. Through the use of a gating system and piston pressure, melted metal is enforced into a die containing a prepared dispersion phase (particles, fibers, or woven material) in order to infiltrate the preform. Figure 22 displays a schematic of the procedure. The molded part is ejected by ejector pins once liquid metal becomes solidified in the mold.

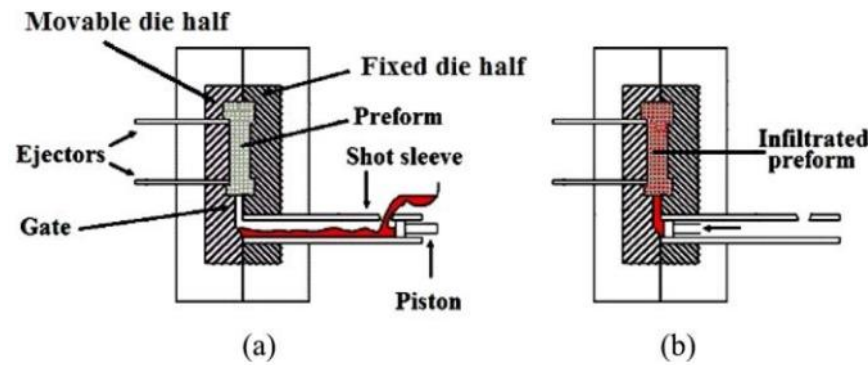


Figure 22. Brief outlines of pressure die infiltration, (a) before infiltration and (b) after infiltration [82].

This technology has many benefits, but the primary ones are its low cost, high precision, and complexity in fabrication. This permits mass manufacturing of net- or near-net-shaped components using traditional pressure die-casting machinery. A suitable gating system design is vital for sound castings, as demonstrated by Long et al.'s [83] study of the processing parameters and geometry of the gating system on void formation. The partially solidified composite casting is isolated from the pressurized melt reservoir in the injection chamber by virtue of melt solidification being finished first in a traditional narrow gating system, as demonstrated by the authors. Preform damage can be avoided by choosing an infiltration speed that keeps the pressure on the preform during infiltration below its elastic compression strength. They advised less than 100 mm/s for the infiltration of Saffil preforms in their selected infiltration system [82].

In addition, Self-propagating High-temperature Synthesis (SHS) has been used to develop various kinds of composites [81,84–87]. The spontaneous infiltration and SHS stick out owing to their simplicity and cost efficiency, owing to which it is worthwhile to pay increased attention to their development. The forced SHS compaction is a one-stage and energy-saving one, and it makes it possible to use the SHS process both for the synthesis of a ceramic framework and for simultaneous metal melting for forced infiltration into the synthesized framework. SHS has been used in obtaining cermets based on combining the SHS of a porous ceramic framework and a subsequent spontaneous infiltration with a metal melt previously prepared via heating from an external source, which makes it possible to use an amount of the melt sufficient for the complete impregnation of a ceramic framework with no overpressure applied.

Squeeze Casting Infiltration Process

For commercial manufacturing of MMCs, the most widely used technology is squeeze casting infiltration. It is widely accepted that the composites made using this technique have a matrix free of pores. A movable mold component (ram) is used in squeeze casting infiltration, a pressure infiltration technique, to apply mechanical pressure to the molten metal during the liquid state manufacturing of metal matrix composites. The lower fixed mold section has a preform dispersion phase that the molten metal is forced to enter. The applied pressure that is maintained during the matrix metal's solidification process typically varies from roughly 10 to 100 MPa or even higher, and it is typically significantly higher than those in gas pressure infiltration methods. The technique is a straight trans-

lation of the well-known squeeze casting method for molding molten metals that are not reinforced and reinforced metal slurries that are created by dispersion techniques to a near-net shape [88–91].

Figures 23a–c and 24a,b depict the brief descriptions of the two types of squeeze casting infiltration processes, namely direct and indirect squeeze casting infiltration. With the earlier technique, shown in Figure 3, the moving die half first descends, comes into contact with the melt surface, and forces the liquid metal to enter the preform (Figure 23a). The material that has infiltrated then solidifies under pressure in the second step (Figure 23b), and in the third step (Figure 23c), the part is extracted from the die using the ejector pin. The vertical shot sleeve tilts in the later approach initially to take a measured amount of molten metal from a ladle and then it returns to its vertical position (Figure 24a). Molten metal is then forced into the die cavity and the preform by a piston (Figure 24b), and high-pressure intensification is applied at the end of the stroke. The die opens after solidification, allowing the penetrated preform to be extracted [82].

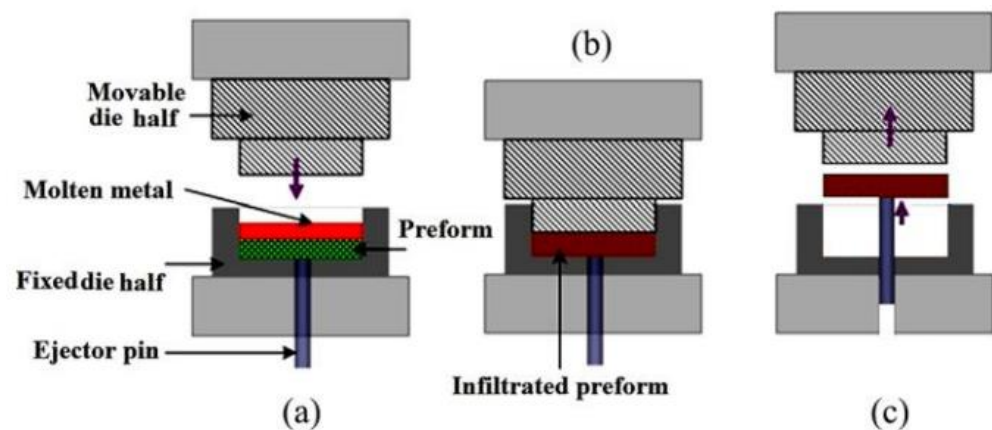


Figure 23. Brief outlines of direct squeeze casting infiltration [82]. (a) the moving die half first descends, comes into contact with the melt surface, and forces the liquid metal to enter the preform, (b) the material that has infiltrated then solidifies under pressure in the second step, (c) in the third step, the part is extracted from the die using the ejector pin.

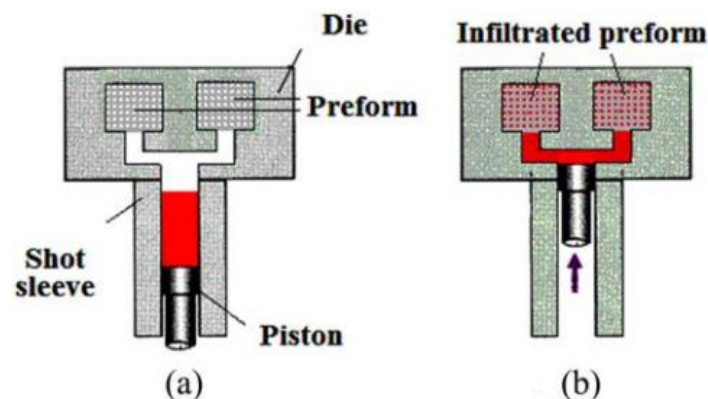


Figure 24. Brief outlines of indirect squeeze casting infiltration [82]. (a) the vertical shot sleeve tilts in the later approach initially to take a measured amount of molten metal from a ladle and then it returns to its vertical position, (b) molten metal is then forced into the die cavity and the preform by a piston.

In addition to being a forced infiltration technique, this one gives the user the option of liquid phase production of metal–metal composites, in which a mold functions as a moveable component and exerts pressure on the metal or molten matrix. The applied pressure and infiltration speed, the reinforcement/melt contact angle, the reinforcement

spacing, the permeability of the preforms, the melt temperature, the die and preform temperatures, and the viscosity and chemistry of the liquid metal are the primary processing parameters for squeeze casting infiltration. The application of pressure to every component of the composite throughout the solidification process, the ease of use of the squeeze casting machine and die, and the almost 100% casting yield are the primary benefits of the squeeze casting infiltration method. Fewer shape restrictions apply to the indirect method. However, the casting yield is lower and the mold and casting machine are more costly and complex [82].

Gas Pressure Infiltration Process

It is also known as pressure infiltration casting (PIC). Aside from the fact that gas is utilized to promote consolidation rather than mechanical pressure, it is comparable to the squeeze casting infiltration method. First created at the Massachusetts Institute of Technology, the fundamental technique of gas pressure infiltration allows for easy and exact control of its process parameters. This method involves applying an inert gas from the outside to the porous preform, allowing the molten metal to seep in [92]. A suitable pressure vessel is used to carry out the melting and metal infiltration. At pressures between 150 and 1500 psi, argon is typically utilized as the inert gas. For aluminum matrix composites, higher pressures have also been studied [93], although safety concerns then become a significant limiting factor [94]. The anti-pressure of the gas can be stated as follows using the ideal gas equation $PV = nRT$:

$$P_g(z) = \frac{P_i T_h L}{T_i (h - z)} \quad (3)$$

where P_i is the pressure of the gas at the initial time, T_h is the temperature of the gas when infiltration attains height h , L is the length of the preform and T_i is the temperature at the initial time.

Figure 25 depicts the schematic of the fundamental gas pressure infiltration procedure. The procedure comes in three different flavors. The first approach involves dipping a heated preform into the melt and forcing the melt to permeate the preform by applying gas pressure to the melt surface. The wettability of the preform, which is a function of the kind and volume percentage of the reinforcement, can be used to determine the gas pressure. Gas pressure is applied to the melt surface in the second variation in the process, forcing the melt up a tube and into the preform. In the third process variant, the preform is positioned in a crucible within the heating chamber, with the metal billet sitting on top of it. Sometimes a small layer of refractory felt is used to cover the preform [82].

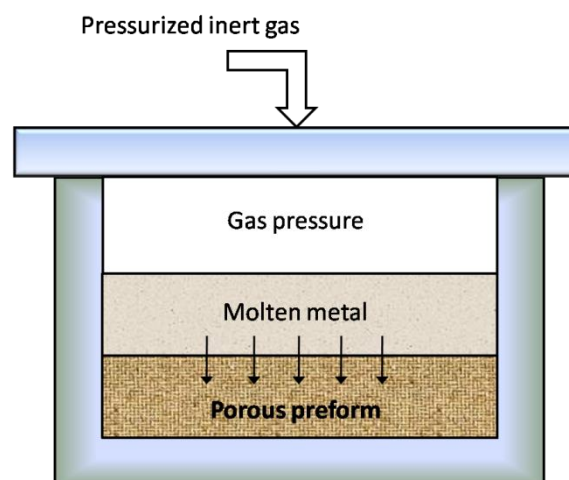


Figure 25. Schematic of gas pressure infiltration process.

Because the reinforcement and the molten metal come into contact quickly during the gas pressure infiltration process, non-coated reinforcements can be used. In comparison to mechanical infiltration procedures, they also cause less damage to the preform. Gas pressure infiltration is extremely controllable for research purposes, but it is not appropriate for high throughput because the pressure chamber must be left open for extended periods of time in order to melt the matrix metal and then cool the composite part after pressure infiltration and solidification are finished [80]. Additionally, there is not much room within the pressure chamber because the insulation and heating components take up a lot of room. The primary characteristic of this procedure is that the preform is heated and the metal is melted outside of the pressure chamber, eliminating the pressure chamber's role as a bottleneck in mass production.

Vacuum Infiltration Process

As illustrated in Figure 26, this method entails negative pressure infiltration, where molten metal is forced into the evacuated preform by applying suction pressure. This method has been applied to the infiltration of aluminum into SiC preforms (AVCO Specialty Materials) and aluminum–lithium alloys into alumina preforms (DuPont) [80]. Process variables including applied vacuum, infiltration temperature, and infiltration time are crucial in the vacuum infiltration process. It is discovered that the infiltration rate increases as the temperature of the molten metal rises. By coating the reinforcement, the interfacial reaction can be avoided and the infiltration incubation period can be shortened [16]. Often, wettability augmentation techniques are employed in tandem with the vacuum infiltration procedure [95]. Molten metal is prevented from entering the pump by filling a section of the connecting pipe with steel chips during the fabrication process. In order to prevent molten metal from becoming trapped in pipes and solidifying in one place without harming the pump, this is carried out.

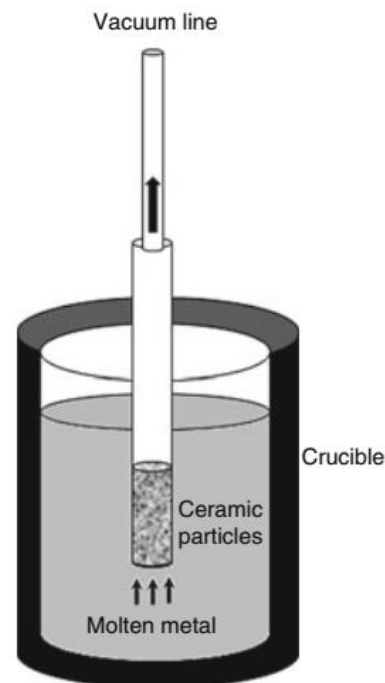


Figure 26. Overview of the vacuum infiltration process [80].

Vacuum infiltration was used by Hajjari et al. [96] to create the Al-Ni coating-based composite reinforced by SiC_p. It is discovered that when infiltration temperature and nickel coating thickness rise, so too does the infiltration rate. As the thickness of the nickel coating increased, the infiltration incubation period reduced. The primary obstacle in the vacuum infiltration process is the produced composite's sluggish rate of solidification,

which promotes grain growth and interfacial interactions between the matrix and reinforcement. The hardness and density of the composites rise as the volume percentage of reinforcement increases. High loads cause a high wear rate; however, as the volume fraction of reinforcement grew, so too did wear resistance [97].

Lorentz Force Infiltration Process

In the new Lorentz force infiltration technique, molten metal is forced into ceramic preforms using electromagnetic force. Throughout the procedure, a high-frequency magnetic pulse is applied to the preform as it is submerged in a liquid molten metal. During the process, the preform position must be suitably oriented with respect to the force axis. A Lorentz body force is developed in the liquid molten metal at the same time as the eddy current generated in the liquid metal interacts with the magnetic pulse, enabling the liquid metal to enter the ceramic rapidly. In this infiltration process, relatively little study has been conducted [98]. The experimental analysis of the Lorentz infiltration process has been extensively studied by Andrews and Mortensen [99]. According to the authors, the increased thickness of the melt ring surrounding the preform was accurately anticipated by the penetrated distance.

Ultrasonic Infiltration Process

Because of their enormous surface-to-volume ratio and low wettability, conventional production procedures like stir casting provide numerous challenges when attempting to combine nano reinforcements into the metal matrix. The approach of spreading nanoparticles in the metal matrix with the help of an ultrasonic probe has proven to be highly effective. Ultrasonic infiltration uses highly transient pressure pulses produced by an ultrasonic probe in contact with the melt to avoid the negative effects of capillary force and wetting challenges [100]. When a horn in the molten metal activates ultrasonic vibration, acoustic cavitation propagates. The cavitation nuclei are created when air is trapped in the porous preform with dissolved gasses in the molten metal. The collapse of bubbles that form near the molten metal causes the infiltration process to happen. High temperatures and shock forces during ultrasonic cavitation break apart the nanoparticle clusters and the nanoparticle reinforcements are uniformly distributed throughout the metal melt to create composites with improved tensile and hardness strength [16].

Centrifugal Infiltration Process

The melt is propelled within the preform by the forces produced by the preform and the melt rotates around an axis during the centrifugal infiltration process. The porous reinforcing material is placed at the end of an extended runner mold that has been filled with molten metal in order to fabricate composites. Excessive runner rotational velocities provide the necessary push for infiltration to surpass the threshold pressure for melt penetration and the viscous forces of the molten metal to flow through the preform. The following formula represents the molten metal pressure that is applied to the porous preform during centrifugal force [98,101]

$$P = \frac{1}{2} \rho \omega^2 (h_2^2 - h_1^2) \quad (4)$$

where ρ is the density of the molten metal, $\omega = (2\pi\Omega/60)$, Ω is the rotational speed (rpm), h_1 is the level of inner molten metal from the rotational axis, h_2 is the level of outer molten metal from the rotational axis.

Centrifugal infiltration is a common technique used to generate near-net form components and prevent material waste. High-pressure centrifugal infiltration is achieved by extending the inner molten metal level h_1 from the rotational axis, which is a minor

alteration made to the same centrifugal system utilized for traditional processes. In these situations, the liquid metal pressure acts on the preform in the following manner [98]:

$$P = \frac{1}{2} \rho \omega^2 h_2^2 \quad (5)$$

As soon as the molten metal begins to seep into the porous preform, the surface pressure of the infiltrated zone drops below the threshold pressure, causing a noticeable reduction in pressure. Since the pressure in the infiltrated zone drops below the threshold pressure, the adhesion between the molten metal and the reinforcement will not separate. In order to attain total molten metal infiltration over the porous preform, it is necessary for the pressure on the infiltration front to surpass the threshold pressure [102].

3.3.5. In Situ Processing

A wide range of methods can be used to produce in situ composite materials. Nonetheless, as illustrated in Figure 27, these procedures can be broadly categorized into two categories: composites produced by solidifying a melt and composites produced by chemical reactions between phases. This method results in the production of the reinforcing phases in the metallic matrix due to in situ chemical reactions between elements or between elements and compounds during the composite fabrication process. A limited number of these alloys were used because of issues with poor growth rates and gradual coarsening of the structure at high temperatures. In situ composites were first used to produce alloys by directional solidification for optics and electronics applications [16,80]. Figures 28 and 29 provide schematic illustrations of in situ processes.

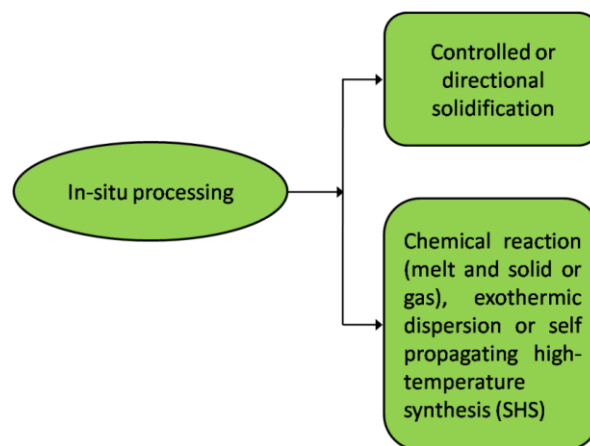


Figure 27. In situ process classification.

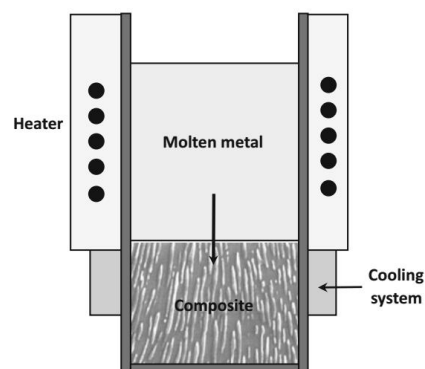


Figure 28. In situ processing by controlled unidirectional solidification of a eutectic alloy [80].

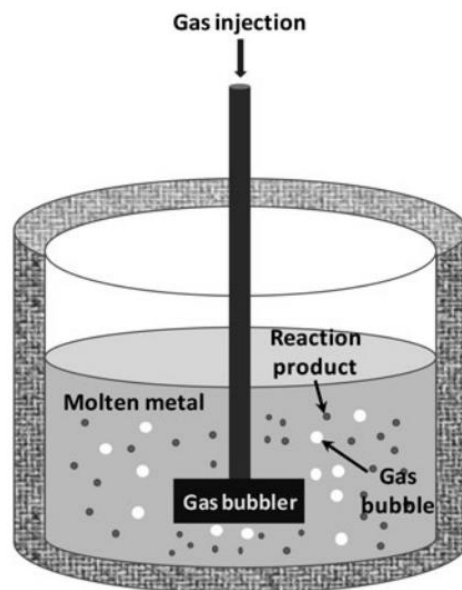


Figure 29. In situ processing by chemical reaction process (gas-molten metal) [80].

A uniform distribution of reinforcement with a tendency toward fineness and a clean interface with the metallic matrix are features of composites synthesized by in situ techniques that help to strengthen the bond between the reinforcement and the metallic matrix [103]. Among the in situ processing methods established to create MMCs are the direct melt reaction (DMR) procedure, reactive hot pressing (RHP), and self-propagating high-temperature synthesis (SHS). The DMR process is thought to be one of the most promising in situ processing methods for commercial applications because of its ease of use, inexpensive cost, and near-net shape-forming capacity [104].

The homogenous distribution of the reinforcing phase and the ability to modify the reinforcement's size or spacing in various situations through reaction time or solidification are two of the main benefits of in situ composite materials. As a result of the constituent phases crystallizing in situ rather than combining from different sources, the interfaces are clean and compatible. On the other hand, little control can be had over the process kinetics, or the form of the reinforcing phases, and there are restrictions on the systems that may be used and the orientation of the reinforcement [80].

The processing of in situ TiB_2 reinforcement in Al alloys started in the early 1990s for the preparation of grain refiners. Many researchers have since synthesized in situ TiB_2 -reinforced composites via K_2TiF_6 and KBF_4 salt reactions in Al alloys [105,106]. A number of researchers have reported the presence of the Al_3Ti phase in Al- TiB_2 composites, which is found to degrade the overall mechanical properties of the composite [107,108]. Later, it was found that Al_3Ti formation can be suppressed by increasing the reaction time and temperature and properly controlling the proportion of salts [106,109,110]. Mandal et al. [106] reported that a melt temperature of $800\text{ }^\circ\text{C}$ and reaction time of 1 h with stirring at an interval of 10 min was optimum for the synthesis of these composites without any Al_3Ti formation. Murty et al. [111] synthesized Al-5 TiB_2 composite by the addition of K_2TiF_6 and KBF_4 salt at $800\text{ }^\circ\text{C}$ and Al-3.45Ti and Al-1.55B master alloy addition at $1000\text{ }^\circ\text{C}$ with 60 min reaction time and observed salt addition results in the formation of more Al_3Ti comparing with the master alloy addition. Al- TiB_2 composites can also be synthesized by a self-propagating high-temperature synthesis (SHS) reaction in an AlTi-B powder compact/preform added to molten Al [112,113]. Yang et al. [112] synthesized Al- TiB_2 composites by the addition of Al-Ti-B powder preform to the molten Al at $900\text{ }^\circ\text{C}$ and studied the mechanism of formation of TiB_2 . They observed that for a Ti:B ratio of 1:2 (mole fraction) in the preform, the TiB_2 particulates formed were spherical in shape. To suppress the Al_3Ti phase, a Ti:B ratio of 1:4 was required.

4. Influence of Process Parameter of Properties

Aluminum matrix composites (AMCs) represent advanced materials renowned for their superior mechanical properties when juxtaposed with conventional aluminum alloys. The characteristics of AMCs undergo considerable influence from diverse processing parameters applied during composite fabrication. These processing parameters, along with their respective ranges, vary depending on the type of fabrication process utilized. Crucial considerations for enhancing the mechanical properties of AMCs encompass a range of significant processing parameters.

4.1. Type of Reinforcement

The kind of reinforcement added to AMCs greatly affects how strong, heat-resistant, and smooth they are. But sometimes, using particles to strengthen the metal can make it less stretchy, which is not good for making structures. Also, if the wrong particle is used with the metal, it might make the metal weaker instead of stronger. That is why it is important to pick the right way to make AMCs and the right settings for making them. Different types of particles are mixed into the metal to make it stronger. Usually, three main kinds of reinforcement are used in AMCs. They are as follows:

- i Ceramic reinforcement: Ceramic reinforcements enhance the wear resistance and thermal stability of AMCs
 - Silicon Carbide (SiC): SiC is an extensively adopted carbide-based reinforcement in AMCs due to its high elastic modulus, technical maturity, and cost-effectiveness [114]. It improves the stiffness and wear resistance of AMCs, rendering them suitable for high-performance tasks.
 - Alumina (Al₂O₃): Alumina reinforcements provide enhanced thermal conductivity and corrosion resistance to AMCs. They are commonly used in applications requiring elevated temperature performance and chemical stability.
 - Boron Carbide (B₄C): B₄C reinforcements offer exceptional hardness and low density, making them well-suited for lightweight and high-strength AMCs used in aerospace and defense applications.
- ii Metal reinforcement: metal reinforcements enhance their fatigue resistance and electrical conductivity.
 - Titanium (Ti) Particles: Ti particles enhance the strength and toughness of AMCs while reducing their density. They improve the fatigue resistance and load-bearing capacity of AMCs, making them suitable for structural applications.
 - Copper (Cu) Particles: Cu reinforcements improve the electrical conductivity and thermal stability of AMCs. They have been commonly used in electronic packaging and heat sink applications.
 - Magnesium (Mg) Particles: Mg reinforcements contribute to the lightweight nature of AMCs while providing good corrosion resistance. They are used in automotive and aerospace applications where weight reduction is critical.
- iii Carbonaceous reinforcement: Carbonaceous reinforcements offer exceptional strength-to-weight ratio and stiffness, making AMCs suitable for lightweight structural applications.
 - Carbon Fibers: Carbon fibers offer a high strength-to-weight ratio and excellent fatigue resistance. They enhance the stiffness and tensile strength of AMCs, making them suitable for lightweight structural components in aerospace and automotive industries [115].
 - Graphene: Graphene reinforcements impart superior mechanical and electrical properties to AMCs. They improve the wear resistance and thermal conductivity of AMCs, enabling their use in advanced engineering applications.

4.2. Size and Distribution of Reinforcement

In addition to the type of particles, the size and distribution of particles are crucial factors in strengthening composites. Typically, composites with finer particle sizes

demonstrate higher composite strength [116]. Yang et al. [117] conducted a study on three composites with varying strengths of Al-Cu-Mg alloy matrices reinforced by three different sizes of SiC particles, subjected to tensile testing. The authors observed that the yield strength (YS), ultimate strength (UTS), and elongation (EL) obtained from the uniaxial tensile testing varied with particle size and matrix strength, as depicted in Figure 30.

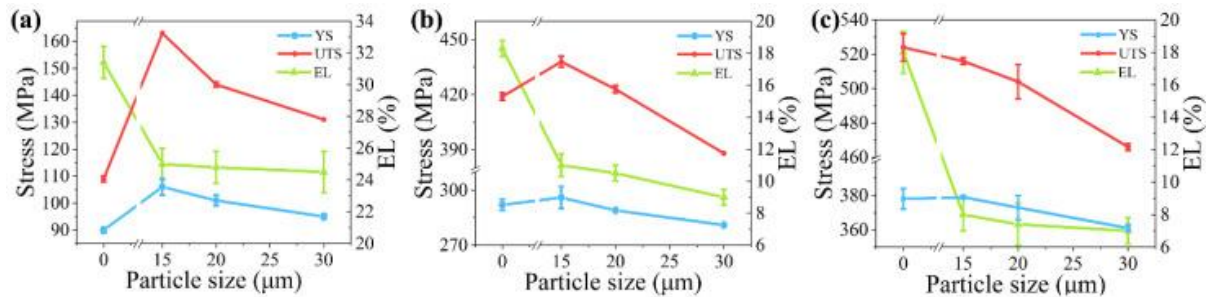


Figure 30. The variation in yield strength (YS), ultimate strength (UTS), and elongation (EL) of the composites with change in matrix type, such as (a) matrix L, (b) matrix M, and (c) matrix H [117]. Chemical compositions in wt. % of Matrix L (Al—100), Matrix M (Cu—2.6, Mg—1.0 Al—balance), Matrix H (Cu—4.2, Mg—1.6 Al—balance).

The effectiveness of a particle is measured by its actual strength, size, shape, and matrix strength. Damage to particles increases with larger particle size [118], higher aspect ratio [119] and stronger matrix materials. In numerical studies, the Weibull law is often utilized for modeling the damage performance of particles [120]. Lewis et al. [119] investigated the occurrence of reinforcement cracking within a particulate under tensile plastic straining. A Weibull modeling method was taken into account to assess the probability of particle cracking. The analytical findings demonstrated close alignment with experimental data for the ZrO₂/2618 Al alloy metal matrix composite. The calculated Weibull modulus denoted as ‘m’ and stress thresholds for particle cracking fell within the anticipated range for ceramic particles.

The Weibull modulus indicates the uniformity of strength values, with higher values indicating greater uniformity. The smaller values of the Weibull modulus correspond to greater variability in strength. Table 3 provides typical ‘m’ values for various reinforcements.

Table 3. Typical Weibull modulus (m) values for materials in fiber form [121,122].

Fiber Materials	Weibull Modulus, m
Glass	<5
Al ₂ O ₃	5–10
Steel	>100
SiC	5, 17
30% zirconia–alumina	21.67

To calculate the overall parameters of the composites, the majority of numerical models of MMCs employed unit cell models with spherical or cylindrical particles [123]. The results of the investigation showed that, for the spherical and cylindrical particle models, the predictions agreed with the experimental findings on the corresponding angular and spherical particle-reinforced composites. Given that the majority of AMCs are made up of angular particles, unit cell models with cylindrical particles would be better appropriate for forecasting the mechanical characteristics of composite materials. In the case of cylindrical particles, the aspect ratio is an important factor for strengthening, load transfer and final mechanical properties. The aspect ratio is generally determined from microstructural analysis of the specific material under consideration. The aspect ratio is characterized by

the ratio of the length to the diameter of the non-spherical reinforcement. These parameters can be calculated by aspect ratio and distribution of particles of experimentally obtained composite material.

These parameters are crucial in determining the mechanical properties of the composite. Christman et al. [124] predicted tensile properties for whiskers with aspect ratios of 4 and 5, and cell aspect ratios of 3, 5, and 6, respectively. The results showed that increasing the cell aspect ratio led to a decrease in the predicted elastic modulus and an increase in the strain-hardening rate, while increasing the whisker aspect ratio enhanced the flow stress. Similarly, Tvergaard [125] found little sensitivity to small changes in the cell aspect ratio, with the whisker aspect ratio having a larger effect on the stress–strain curve. Li et al. [119] investigated the compressive plastic deformation of particle-reinforced metal matrix composites and predicted the flow stress of the composites using different processing conditions. Their results revealed that strain-based properties (flow stress and the strain-rate hardening exponents) increased with the volume fraction of the reinforcement. On the other hand, the rate-dependent flow stress was influenced by both particle morphology (aspect ratio) and particle shape (spheroidal or cylindrical).

4.3. Matrix Material

A diverse range of metals and their alloys serve as matrix materials in MMCs. Metals exhibit metallic bonding characterized by nondirectional electronic bonding, contributing to isotropy in many properties. Metals are crystalline, with ions packed in regular closed-packed arrangements, primarily in face-centered cubic (FCC) and hexagonal close-packed (HCP) structures. A less dense body-centered cubic (BCC) arrangement is also observed in some metals. During the deformation of matrix materials, point defects and line defects become active. Point defects occur in thermal equilibrium, while dislocations, grain boundaries, etc., represent higher energy levels. Dislocations, such as edge and screw dislocations, reduce the force required for the plastic deformation of materials. Matrix metals and alloys can be strengthened through various mechanisms known as strengthening mechanisms.

- I. Dislocation strengthening: Dislocation strengthening occurs when dislocations and their interactions generate internal stress fields, requiring additional force to move a dislocation through these fields. This strengthening effect arises from an increase in dislocation density, often resulting from processes like cold working. In polycrystalline metals, the shear stress needed to move dislocations can be calculated using the following formula,

$$\tau = \tau_0 + \alpha Gb\sqrt{\rho}$$

where τ is shear stress, τ_0 is frictional stress, G is shear modulus, b is burger vector and ρ is dislocation density. The α is a constant.

- II. Grain boundary strengthening: Grain boundary strengthening is significant at moderate temperatures, where grain boundaries serve as effective sources of strengthening. The Hall–Petch equation describes this phenomenon as follows:

$$\sigma_y = \sigma_0 + k/\sqrt{D}$$

where σ_y is yield strength, σ_0 is friction stress, k is the Hall–Petch coefficient and D is the average grain size. However, for nanograins, this equation does not apply, and instead, an inverse Hall–Petch equation is used. The exponent of “ D ” varies with grain size in this scenario.

- III. Precipitation strengthening: Precipitation strengthening involves the presence of precipitates, solute atoms, or dispersoids that hinder dislocation movement, thereby strengthening the matrix. This mechanism is crucial for alloys such as aluminum, nickel, and steel. Precipitation strengthening requires careful control to enhance strength, such as increasing hardness in aluminum-copper alloys through mechanisms like the clustering of Cu atoms on (100) planes of Al.

4.4. Processing Temperature

The processing temperature is closely linked to the chosen processing technique. MMC fabrication can occur in two primary states: liquid and solid. In liquid-state processing, MMCs are formed by blending or combining a liquid metal matrix with the reinforcement. This method offers advantages such as near-net-shape fabrication (compared to solid-state processes like extrusion or diffusion bonding), quicker processing rates, and relatively low temperatures required for melting most light metals like Al and Mg. However, a notable drawback of this approach is the potential for particle segregation, elemental segregation, and the formation of dendritic structures in the final microstructure (Figure 31).

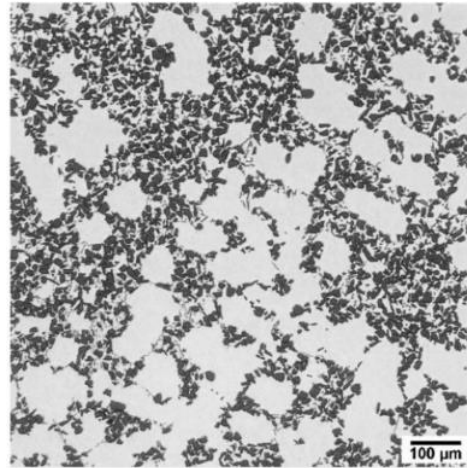


Figure 31. Clustering SiC particles in Al resulting from slow cooling leading to inhomogeneous distribution of particles, due to particle pushing and segregation [126].

Another drawback of liquid-phase processing is the potential for an inhomogeneous distribution of second-phase reinforcements and the development of an uneven matrix microstructure. Additionally, there is a risk of adverse interfacial reactions between reinforcements and matrix materials at elevated temperatures. These challenges associated with liquid-state processing can be addressed by solid-phase processes, in which the processing temperature is significantly less compared to the melting temperature of matrix materials in MMCs. In powder metallurgy processing, cold pressing and sintering or hot pressing techniques are employed for fabricating MMCs with higher densification. On the other hand, roll bonding is utilized to produce laminate composites comprising different layers with distinct materials (Figure 32). Roll bonding can also be combined with hot pressing to create laminates consisting of Al sheets and discontinuously reinforced MMCs [127].

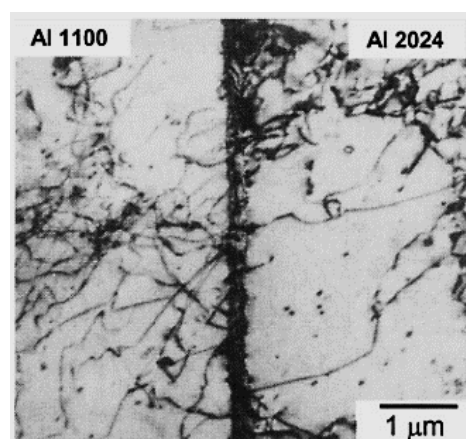


Figure 32. TEM of a roll-bonded Al 1100 and Al 2024 laminated composite, showing good interface interaction [121].

5. Application of AMCs

Aluminum metal composites (AMCs) have found extensive commercial use across various industrial sectors, including aerospace, automotive, and structural component fabrication [104]. AMCs provide an exceptional combination of physical and mechanical properties. Alongside metallic alloys from which they are derived, these composites exhibit high electrical conductivity and thermal, higher stability to harsh environments, improved impact and erosion resistance, and creditable fatigue and fracture properties [128]. In automotive applications, AMCs are utilized to develop disc brake rotors, cylinder bores in engines, and drive shafts (Figure 33).

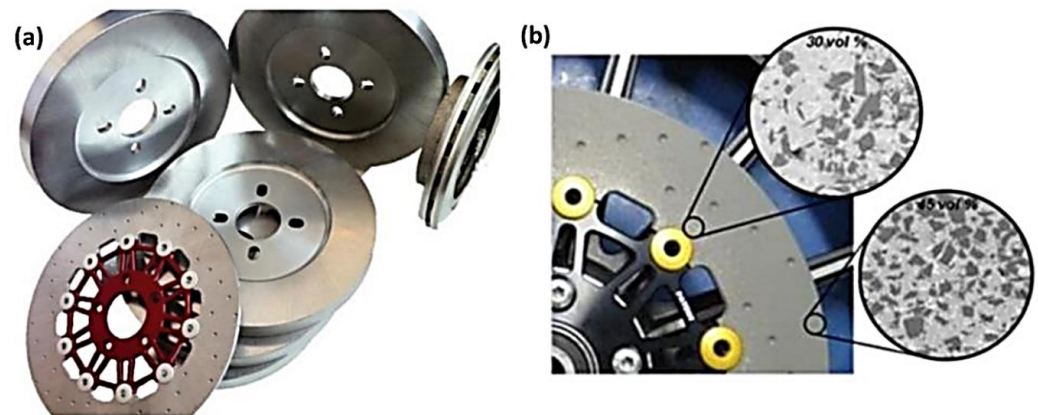


Figure 33. (a) Brake rotors made of Al MMCs and (b) A gradient microstructure with high ceramic loading on the outer periphery where the disc moves fastest and generates maximum heat and lower loading inward to maintain [11,128].

Honda manufactures cylinder bores by infiltrating preforms composed of chopped Saffil and graphite fibers. Comparable methods are employed for creating selectively reinforced cylinder bores for the Porsche Boxster and 911 Carrera models (Figure 34). Notably, the commercial automotive market witnessed a significant milestone with the introduction of selectively reinforced pistons manufactured using liquid metal infiltration for Toyota diesel engines in 1983 [129]. Building on this success, Honda adopted selectively reinforced engine cylinder bores in 1990 (Figure 3). Honda's pioneering approach involves a straightforward process for creating ceramic preforms for cylinder bores using chopped Saffil and graphite fibers, seamlessly integrating preform infiltration into the engine block casting process. This innovative technique is nowadays widely utilized in various Honda vehicles, including the Prelude SI, the Honda Accord, and the V6 engine of the Acura NSX and S2000 Roadster.

AMCs have found application in space systems, with examples including tubes made of 6061 Al reinforced by monofilaments applicable in the space shuttle orbiter, and tows made of 6061Al/Gr fiber composite utilized for the Hubble Space Telescope antenna waveguide mast. In aeronautics, MMC applications span various categories, including aerostructural, aero-propulsion, and subsystems. In the aerostructural category, MMCs are employed in components such as ventral fins (Figure 35) and fuel access door covers on F-16 aircraft. Moreover, rotor blade sleeves and swashplates on helicopters like the Eurocopter EC120 and N4 also incorporate MMCs. These applications highlight the versatility and efficacy of MMCs in enhancing the performance and durability of aeronautical components.

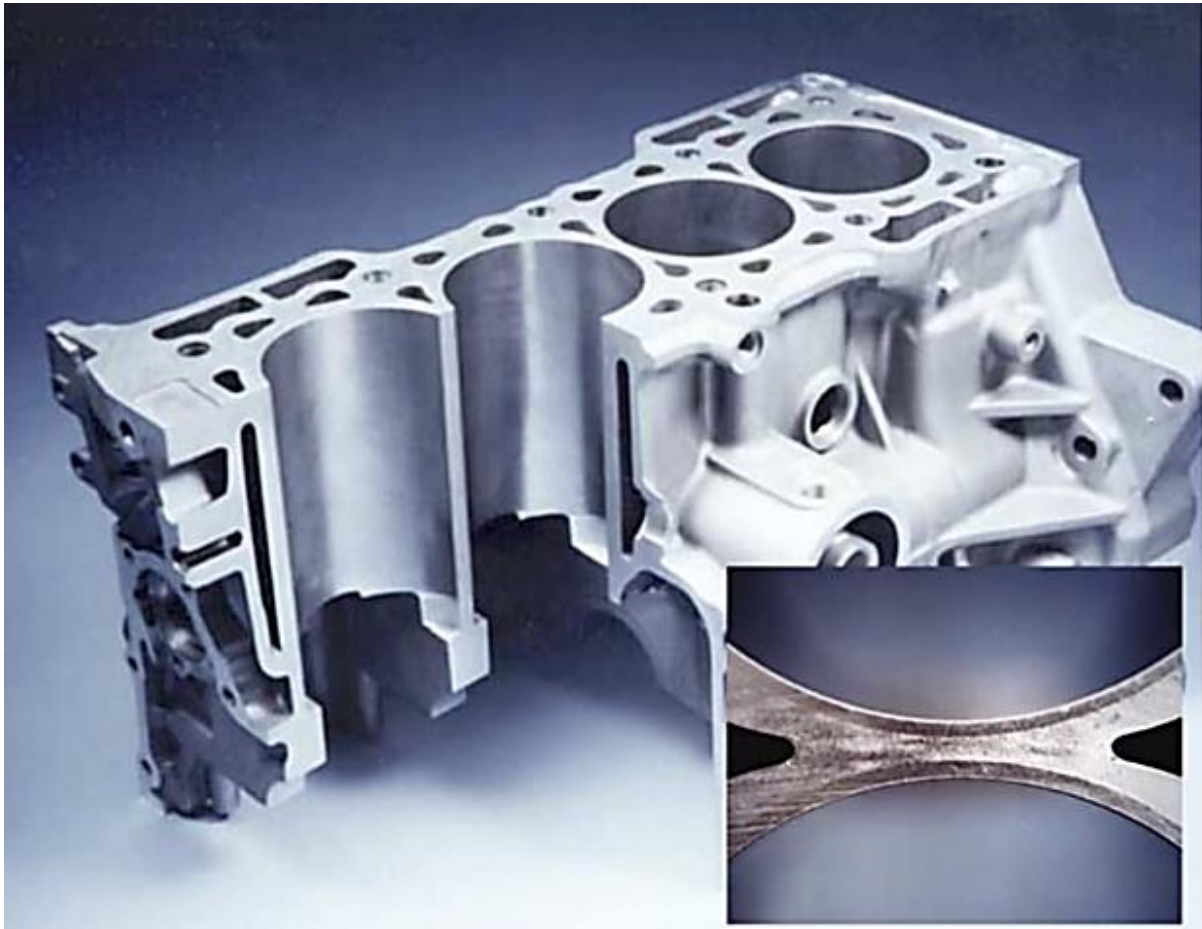


Figure 34. Honda Prelude 2.0 l cast aluminum cylinder block with an inset showing the selective reinforcement for the cylinder liner [129].



Figure 35. The F-16 features ventral fins positioned on the bottom of the fuselage, aft (rearward) of the wings. These ventral fins serve the purpose of stabilizing the aircraft during high-angle ascents and other maneuvers. However, the original design of the ventral fins experienced aerodynamic buffeting, resulting in a high failure rate [130].

AMC components find applications in the recreational market as well as in infrastructure projects. In the recreational market, AMCs are utilized in various products such as bicycle tubing, track spikes, and lacrosse stick shafts. These components benefit from the enhanced strength, stiffness, and lightweight properties offered by AMCs, leading to improved performance and durability in recreational activities. In infrastructure projects, AMCs are essential, particularly in nuclear waste containment and overhead power transmission conductors. For instance, Al/B₄C AMCs are chosen for nuclear waste containment because of their high microstructural stability, compressive strength and corrosion resistance. The transmission lines feature 3M aluminum conductor composite-reinforced high-capacity transmission conductors, consisting of an AMC core surrounded by Al-Zr outer wires (refer to Figure 36). These conductors are lightweight and anticipated to deliver a substantial increase in power-carrying capacity, ranging from 200% to 300% [11].



Figure 36. The cross-section of a 3M aluminum conductor composite-reinforced (ACCR) high-capacity MMC conductor used in overhead transmission lines consists of an aluminum core surrounded by Al-Zr outer wires. This design enhances strength, stiffness, and current-carrying capacity while minimizing weight and maximizing conductivity [11].

6. Conclusions and Future Directions

Improvement in processing and reduction in intrinsic cost remain important aspects for the commercialization of AMCs. Application of engineering design and modeling the directionality of reinforcement is necessary to achieve the full potential of composite structures. In addition, online monitoring of manufacturing processes and online health monitoring of AMCs are expected to provide additional benefits in terms of commercialization of the process. Therefore, research and development opportunities remain the primary objective for the development of any new composite structure. Research to compute the effect of reinforced particle size, morphology and distribution is an important consideration while developing AMCs with higher strength, stiffness and ductility. Continuously reinforced Al/Al₂O₃ MMCs have seen commercial applications in aerospace domains [131]. Uniaxial applications like tubes, struts, and hoop components are feasible, with selective reinforcement proving to be an effective strategy. By integrating novel procedures, wire or tape preforms of this material may be utilized for constructing industrial structures. This method permits the creation of tailored parts with enhanced mechanical characteristics, offering versatility and adaptability in various engineering applications. It is noted that many MMC materials remain at an inception stage, offering tremendous openings for upcoming research and development of second-generation MMC materials. Shape

memory alloys and magnetic metals can be promising candidates for multifunctional MMC applications. The importance of exploring composite architectures, including bimodal reinforcement sizes and intentional inhomogeneity, to unlock new possibilities in MMC design and performance needs to be revised and explored.

Finally, the potential of foam architectures to expand MMC applications beyond traditional structural uses to areas such as sound isolation, blast protection, and thermal management is required to be investigated for niche applications such as sound isolation, blast and crash protection, fire protection and thermal transfer properties that range from heat exchangers to thermal insulators. Valuable insights have emerged from recent studies on composite processes and designs, offering valuable guidance for the future advancement of AMCs. Ongoing research endeavors aim to enhance current MMC materials and techniques while also exploring novel metals and architectures for the development of a second generation of MMCs.

Author Contributions: A.K.: conceptualization, methodology, validation, formal analysis, writing—original draft preparation, writing—review and editing, A.S.: writing—original draft preparation, writing—review and editing, S.K.: conceptualization, methodology, project administration, writing—review and editing, funding acquisition, supervision. All authors have read and agreed to the published version of the manuscript.

Funding: This research received no external funding.

Institutional Review Board Statement: Not applicable.

Data Availability Statement: No new data was created or analyzed in this work. Data sharing is not applicable to this work.

Conflicts of Interest: The authors declare no conflicts of interest. The authors declare that they have no known competing financial interests or personal relationships that could have appeared to influence the work reported in this paper.

References

- Kok, M. Production and mechanical properties of Al₂O₃ particle-reinforced 2024 aluminium alloy composites. *J. Mater. Process. Technol.* **2005**, *161*, 381–387. [\[CrossRef\]](#)
- Lee, H.S.; Yeo, J.S.; Hong, S.H.; Yoon, D.J.; Na, K.H. The fabrication process and mechanical properties of SiC_p/Al–Si metal matrix composites for automobile air-conditioner compressor pistons. *J. Mater. Process. Technol.* **2001**, *113*, 202–208. [\[CrossRef\]](#)
- Rohatgi, P.K.; Asthana, R.; Das, S. Solidification, structures, and properties of cast metal-ceramic particle composites. *Int. Met. Rev.* **1986**, *31*, 115–139. [\[CrossRef\]](#)
- Kumar, S.; Adarsh, D.; Kailas, S.V. Fabrication and tribo characteristics of in-situ polymer-derived nano-ceramic composites of Al–Mg–Si alloy. *Tribol. Int.* **2023**, *180*, 108272. [\[CrossRef\]](#)
- Yanming, Q.; Zehua, Z. Tool wear and its mechanism for cutting SiC particle-reinforced aluminium matrix composites. *J. Mater. Process. Technol.* **2000**, *100*, 194–199. [\[CrossRef\]](#)
- Surappa, M.K. Aluminium matrix composites: Challenges and opportunities. *Sadhana-Acad. Proc. Eng. Sci.* **2003**, *28*, 319–334.
- Olszówka-Myalska, A.; Szala, J.; Cwajna, J. Characterization of reinforcement distribution in Al/(Al₂O₃)_p composites obtained from composite powder. *Mater. Charact.* **2001**, *46*, 189–195. [\[CrossRef\]](#)
- Bains, P.S.; Sidhu, S.S.; Payal, H.S. Fabrication and Machining of Metal Matrix Composites: A Review. *Mater. Manuf. Process.* **2016**, *31*, 553–573. [\[CrossRef\]](#)
- Schwartz, M. Composite Materials: Processing, fabrication. *Prentice Hall* **1997**, *2*.
- Vani, V.V.; Chak, S.K. The effect of process parameters in Aluminum Metal Matrix Composites with Powder Metallurgy. *Manuf. Rev.* **2018**, *5*, 7. [\[CrossRef\]](#)
- Miracle, D.B. Metal matrix composites—From science to technological significance. *Compos. Sci. Technol.* **2005**, *65*, 2526–2540. [\[CrossRef\]](#)
- Rajmohan, T.; Palanikumar, K.; Arumugam, S. Synthesis and characterization of sintered hybrid aluminium matrix composites reinforced with nanocopper oxide particles and microsilicon carbide particles. *Compos. Part B Eng.* **2014**, *59*, 43–49. [\[CrossRef\]](#)
- Slipenyuk, A.; Kuprin, V.; Milman, Y.; Spowart, J.E.; Miracle, D.B. The effect of matrix to reinforcement particle size ratio (PSR) on the microstructure and mechanical properties of a P/M processed AlCuMn/SiC_p MMC. *Mater. Sci. Eng. A* **2004**, *381*, 165–170. [\[CrossRef\]](#)
- Kumar, S.; Kar, A. A Review of Solid-State Additive Manufacturing Processes. *Trans. Indian Natl. Acad. Eng.* **2021**, *6*, 955–973. [\[CrossRef\]](#)
- Casati, R.; Vedani, M. Metal matrix composites reinforced by nano-particles—A review. *Metals* **2014**, *4*, 65–83. [\[CrossRef\]](#)

16. Garg, P.; Jamwal, A.; Kumar, D.; Sadasivuni, K.K.; Hussain, C.M.; Gupta, P. Advance Research Progresses in Aluminium Matrix Composites: Manufacturing & Applications. *J. Mater. Res. Technol.* **2019**, *8*, 4924–4939. [[CrossRef](#)]
17. Khedr, M.; Hamada, A.; Järvenpää, A.; Elkatatny, S.; Abd-Elaziem, W. Review on the Solid-State Welding of Steels: Diffusion Bonding and Friction Stir Welding Processes. *Metals* **2023**, *13*, 54. [[CrossRef](#)]
18. Zhang, X.P.; Ye, L.; Mai, Y.W.; Quan, G.F.; Wei, W. Investigation on diffusion bonding characteristics of SiC particulate reinforced aluminium metal matrix composites (Al/SiC_p-MMC). *Compos. Part A Appl. Sci. Manuf.* **1999**, *30*, 1415–1421. [[CrossRef](#)]
19. Abubaker, H.M.; Merah, N.; Al-badour, F.A.; Albinmoussa, J.; Sorour, A.A. Influence of Friction Stir Processing on Mechanical Behavior of 2507 SDSS. *Metals* **2020**, *10*, 369. [[CrossRef](#)]
20. Mironov, S.; Sato, Y.S.; Kokawa, H. Microstructural evolution during friction stir-processing of pure iron. *Acta Mater.* **2008**, *56*, 2602–2614. [[CrossRef](#)]
21. McNelley, T.R.; Swaminathan, S.; Su, J.Q. Recrystallization mechanisms during friction stir welding/processing of aluminum alloys. *Scr. Mater.* **2008**, *58*, 349–354. [[CrossRef](#)]
22. Mirjavadi, S.S.; Alipour, M.; Emamian, S.; Kord, S.; Hamouda, A.M.S.; Koppad, P.G.; Keshavamurthy, R. Influence of TiO₂ nanoparticles incorporation to friction stir welded 5083 aluminum alloy on the microstructure, mechanical properties and wear resistance. *J. Alloys Compd.* **2017**, *712*, 795–803. [[CrossRef](#)]
23. Kumar, S.; Wu, C.S.; Sun, Z.; Ding, W. Effect of ultrasonic vibration on welding load, macrostructure, and mechanical properties of Al/Mg alloy joints fabricated by friction stir lap welding. *Int. J. Adv. Manuf. Technol.* **2019**, *100*, 1787–1799. [[CrossRef](#)]
24. Kumar, S.; Ding, W.; Sun, Z.; Wu, C.S. Analysis of the dynamic performance of a complex ultrasonic horn for application in friction stir welding. *Int. J. Adv. Manuf. Technol.* **2018**, *97*, 1269–1284. [[CrossRef](#)]
25. Kumar, S.; Wu, C.S. A novel technique to join Al and Mg alloys: Ultrasonic vibration assisted linear friction stir welding. *Mater. Today Proc.* **2018**, *5*, 18142–18151. [[CrossRef](#)]
26. Akramifard, H.R.; Shamanian, M.; Sabbaghian, M.; Esmailzadeh, M. Microstructure and mechanical properties of Cu/SiC metal matrix composite fabricated via friction stir processing. *Mater. Des.* **2014**, *54*, 838–844. [[CrossRef](#)]
27. Lim, D.K.; Shibayanagi, T.; Gerlich, A.P. Synthesis of multi-walled CNT reinforced aluminium alloy composite via friction stir processing. *Mater. Sci. Eng. A* **2009**, *507*, 194–199. [[CrossRef](#)]
28. Azarsa, E.; Mostafapour, A. On the feasibility of producing polymer-metal composites via novel variant of friction stir processing. *J. Manuf. Process.* **2013**, *15*, 682–688. [[CrossRef](#)]
29. Ajay Kumar, P.; Raj, R.; Kailas, S.V. A novel in-situ polymer derived nano ceramic MMC by friction stir processing. *Mater. Des.* **2015**, *85*, 626–634. [[CrossRef](#)]
30. Cao, X.; Shi, Q.; Liu, D.; Feng, Z.; Liu, Q.; Chen, G. Fabrication of in situ carbon fiber/aluminum composites via friction stir processing: Evaluation of microstructural, mechanical and tribological behaviors. *Compos. Part B Eng.* **2018**, *139*, 97–105. [[CrossRef](#)]
31. Iijima, K.; Terashima, T.; Yamamoto, K.; Hirata, K.; Bando, Y. Preparation of ferroelectric BaTiO₃ thin films by activated reactive evaporation. *Appl. Phys. Lett.* **1990**, *56*, 527–529. [[CrossRef](#)]
32. Wang, Y.; Chen, W.; Wang, B.; Zheng, Y. Ultrathin Ferroelectric Films: Growth, Characterization, Physics and Applications. *Materials* **2014**, *7*, 6377–6485. [[CrossRef](#)] [[PubMed](#)]
33. Rabe, K.; Ahn, C.; Triscone, J. *Physics of Ferroelectrics: A Modern Perspective*; Springer: Berlin/Heidelberg, Germany, 2007; Volume 105, p. 388.
34. Dadbakhsh, S.; Mertens, R.; Hao, L.; Van Humbeeck, J.; Kruth, J.P. Selective Laser Melting to Manufacture “In Situ” Metal Matrix Composites: A Review. *Adv. Eng. Mater.* **2019**, *21*, 1801244. [[CrossRef](#)]
35. Wang, P.; Eckert, J.; Prashanth, K.-G.; Wu, M.-W.; Kaban, I.; Xi, L.-X.; Scudino, S. A review of particulate-reinforced aluminum matrix composites fabricated by selective laser melting. *Trans. Nonferrous Met. Soc. China* **2020**, *30*, 2001–2034. [[CrossRef](#)]
36. Wang, P.; Zhang, B.; Tan, C.C.; Raghavan, S.; Lim, Y.F.; Sun, C.N.; Wei, J.; Chi, D. Microstructural characteristics and mechanical properties of carbon nanotube reinforced Inconel 625 parts fabricated by selective laser melting. *Mater. Des.* **2016**, *112*, 290–299. [[CrossRef](#)]
37. Yuan, P.; Gu, D.; Dai, D. Particulate migration behavior and its mechanism during selective laser melting of TiC reinforced Al matrix nanocomposites. *Mater. Des.* **2015**, *82*, 46–55. [[CrossRef](#)]
38. Gu, D.; Wang, H.; Dai, D.; Yuan, P.; Meiners, W.; Poprawe, R. Rapid fabrication of Al-based bulk-form nanocomposites with novel reinforcement and enhanced performance by selective laser melting. *Scr. Mater.* **2015**, *96*, 25–28. [[CrossRef](#)]
39. Simchi, A.; Godlinski, D. Effect of SiC particles on the laser sintering of Al–7Si–0.3Mg alloy. *Scr. Mater.* **2008**, *59*, 199–202. [[CrossRef](#)]
40. Liao, H.; Zhu, H.; Xue, G.; Zeng, X. Alumina loss mechanism of Al₂O₃-AlSi₁₀ Mg composites during selective laser melting. *J. Alloys Compd.* **2019**, *785*, 286–295. [[CrossRef](#)]
41. What is Directed Energy Deposition (DED)?—TWI. Available online: <https://www.twi-global.com/technical-knowledge/faqs/directed-energy-deposition> (accessed on 21 March 2024).
42. Hu, Y.; Cong, W. A review on laser deposition-additive manufacturing of ceramics and ceramic reinforced metal matrix composites. *Ceram. Int.* **2018**, *44*, 20599–20612. [[CrossRef](#)]
43. Balla, V.K.; Bose, S.; Bandyopadhyay, A. Processing of Bulk Alumina Ceramics Using Laser Engineered Net Shaping. *Int. J. Appl. Ceram. Technol.* **2008**, *5*, 234–242. [[CrossRef](#)]

44. Li, Y.; Hu, Y.; Cong, W.; Zhi, L.; Guo, Z. Additive manufacturing of alumina using laser engineered net shaping: Effects of deposition variables. *Ceram. Int.* **2017**, *43*, 7768–7775. [[CrossRef](#)]
45. Wu, D.; Sun, B.; Niu, F.; Ma, G.; Zhang, Y.; Jin, Z. Microstructure and crack in color Al₂O₃ samples by laser engineered net shaping. *Kuei Suan Jen Hsueh Pao/J. Chin. Ceram. Soc.* **2013**, *41*, 1621–1626.
46. Niu, F.; Wu, D.; Zhou, S.; Ma, G. Power prediction for laser engineered net shaping of Al₂O₃ ceramic parts. *J. Eur. Ceram. Soc.* **2014**, *34*, 3811–3817. [[CrossRef](#)]
47. Niu, F.; Wu, D.; Ma, G.; Wang, J.; Guo, M.; Zhang, B. Nanosized microstructure of Al₂O₃–ZrO₂ (Y₂O₃) eutectics fabricated by laser engineered net shaping. *Scr. Mater.* **2015**, *95*, 39–41. [[CrossRef](#)]
48. Yan, S.; Wu, D.; Niu, F.; Ma, G.; Kang, R. Al₂O₃–ZrO₂ eutectic ceramic via ultrasonic-assisted laser engineered net shaping. *Ceram. Int.* **2017**, *43*, 15905–15910. [[CrossRef](#)]
49. Hu, Y.; Ning, F.; Cong, W.; Li, Y.; Wang, X.; Wang, H. Ultrasonic vibration-assisted laser engineering net shaping of ZrO₂–Al₂O₃ bulk parts: Effects on crack suppression, microstructure, and mechanical properties. *Ceram. Int.* **2018**, *44*, 2752–2760. [[CrossRef](#)]
50. Champagne, V.; Helfritch, D. The unique abilities of cold spray deposition. *Int. Mater. Rev.* **2016**, *61*, 437–455. [[CrossRef](#)]
51. Vilardell, A.M.; Cinca, N.; Concustell, A.; Dosta, S.; Cano, I.G.; Guilemany, J.M. Cold spray as an emerging technology for biocompatible and antibacterial coatings: State of art. *J. Mater. Sci.* **2015**, *50*, 4441–4462. [[CrossRef](#)]
52. Champagne, V.K.; Helfritch, D.J. Mainstreaming cold spray—Push for applications. *Surf. Eng.* **2014**, *30*, 396–403. [[CrossRef](#)]
53. Kar, A.; Kumar, S.; Kailas, S.V. Developing multi-layered 3D printed homogenized structure using solid state deposition method. *Mater. Charact.* **2023**, *199*, 112770. [[CrossRef](#)]
54. Yin, S.; Aldwell, B.; Lupoi, R. Cold spray additive manufacture and component restoration. In *Cold-Spray Coatings: Recent Trends and Future Perspectives*; Springer International Publishing: Cham, Switzerland, 2017; pp. 195–224. [[CrossRef](#)]
55. Raelison, R.N.; Xie, Y.; Sapanathan, T.; Planche, M.P.; Kromer, R.; Costil, S.; Langlade, C. Cold gas dynamic spray technology: A comprehensive review of processing conditions for various technological developments till to date. *Addit. Manuf.* **2018**, *19*, 134–159. [[CrossRef](#)]
56. Yin, S.; Cavaliere, P.; Aldwell, B.; Jenkins, R.; Liao, H.; Li, W.; Lupoi, R. Cold spray additive manufacturing and repair: Fundamentals and applications. *Addit. Manuf.* **2018**, *21*, 628–650. [[CrossRef](#)]
57. Li, W.; Yang, K.; Yin, S.; Yang, X.; Xu, Y.; Lupoi, R. Solid-state additive manufacturing and repairing by cold spraying: A review. *J. Mater. Sci. Technol.* **2018**, *34*, 440–457. [[CrossRef](#)]
58. Wang, X.; Feng, F.; Klecka, M.A.; Mordasky, M.D.; Garofano, J.K.; El-Wardany, T.; Nardi, A.; Champagne, V.K. Characterization and modeling of the bonding process in cold spray additive manufacturing. *Addit. Manuf.* **2015**, *8*, 149–162. [[CrossRef](#)]
59. Li, W.Y.; Li, C.J.; Liao, H. Significant influence of particle surface oxidation on deposition efficiency, interface microstructure and adhesive strength of cold-sprayed copper coatings. *Appl. Surf. Sci.* **2010**, *256*, 4953–4958. [[CrossRef](#)]
60. Chen, C.; Xie, Y.; Yan, X.; Yin, S.; Fukanuma, H.; Huang, R.; Zhao, R.; Wang, J.; Ren, Z.; Liu, M.; et al. Effect of hot isostatic pressing (HIP) on microstructure and mechanical properties of Ti6Al4V alloy fabricated by cold spray additive manufacturing. *Addit. Manuf.* **2019**, *27*, 595–605. [[CrossRef](#)]
61. Ma, W.; Xie, Y.; Chen, C.; Fukanuma, H.; Wang, J.; Ren, Z.; Huang, R. Microstructural and mechanical properties of high-performance Inconel 718 alloy by cold spraying. *J. Alloys Compd.* **2019**, *792*, 456–467. [[CrossRef](#)]
62. Gärtner, F.; Stoltenhoff, T.; Voyer, J.; Kreye, H.; Riekehr, S.; Koçak, M. Mechanical properties of cold-sprayed and thermally sprayed copper coatings. *Surf. Coat. Technol.* **2006**, *200*, 6770–6782. [[CrossRef](#)]
63. Binder, K.; Gottschalk, J.; Kollenda, M.; Gärtner, F.; Klassen, T. Influence of Impact Angle and Gas Temperature on Mechanical Properties of Titanium Cold Spray Deposits. *J. Therm. Spray Technol.* **2010**, *20*, 234–242. [[CrossRef](#)]
64. Meydanoglu, O.; Jodoin, B.; Kayali, E.S. Microstructure, Mechanical Properties and Corrosion Performance of 7075 Al Matrix Ceramic Particle Reinforced Composite Coatings Produced by the Cold Gas Dynamic Spraying Process. *Surf. Coatings Technol.* **2013**, *235*, 108–116. [[CrossRef](#)]
65. Yu, M.; Suo, X.K.; Li, W.Y.; Wang, Y.Y.; Liao, H.L. Microstructure, mechanical property and wear performance of cold sprayed Al₅₀₅₆/SiC_p composite coatings: Effect of reinforcement content. *Appl. Surf. Sci.* **2014**, *289*, 188–196. [[CrossRef](#)]
66. Qiu, X.; Tariq, N.U.H.; Wang, J.-Q.; Tang, J.-R.; Gyansah, L.; Zhao, Z.-P.; Xiong, T.-Y. Microstructure, microhardness and tribological behavior of Al₂O₃ reinforced A380 aluminum alloy composite coatings prepared by cold spray technique. *Surf. Coat. Technol.* **2018**, *350*, 391–400. [[CrossRef](#)]
67. Yang, X.; Li, W.; Yu, S.; Xu, Y.; Hu, K.; Zhao, Y. Electrochemical characterization and microstructure of cold sprayed AA5083/Al₂O₃ composite coatings. *J. Mater. Sci. Technol.* **2020**, *59*, 117–128. [[CrossRef](#)]
68. Tariq, N.H.; Gyansah, L.; Wang, J.Q.; Qiu, X.; Feng, B.; Siddique, M.T.; Xiong, T.Y. Cold spray additive manufacturing: A viable strategy to fabricate thick B4C/Al composite coatings for neutron shielding applications. *Surf. Coat. Technol.* **2018**, *339*, 224–236. [[CrossRef](#)]
69. Kumar, S.; Reddy, S.K.; Joshi, S.V. Microstructure and performance of cold sprayed Al-SiC composite coatings with high fraction of particulates. *Surf. Coat. Technol.* **2017**, *318*, 62–71. [[CrossRef](#)]
70. Xie, X.; Chen, C.; Chen, Z.; Wang, W.; Yin, S.; Ji, G.; Liao, H. Achieving Simultaneously Improved Tensile Strength and Ductility of a Nano-TiB₂/AlSi₁₀Mg Composite Produced by Cold Spray Additive Manufacturing. *Compos. Part B Eng.* **2020**, *202*, 108404. [[CrossRef](#)]

71. Bourkhani, R.D.; Eivani, A.R.; Nateghi, H.R. Through-thickness inhomogeneity in microstructure and tensile properties and tribological performance of friction stir processed AA1050-Al₂O₃ nanocomposite. *Compos. Part B Eng.* **2019**, *174*, 107061. [[CrossRef](#)]
72. Kala, H.; Mer, K.K.S.; Kumar, S. A Review on Mechanical and Tribological Behaviors of Stir Cast Aluminum Matrix Composites. *Procedia Mater. Sci.* **2014**, *6*, 1951–1960. [[CrossRef](#)]
73. Prasad, M.G.A.; Bandekar, N.; Prasad, M.G.A.; Bandekar, N. Study of Microstructure and Mechanical Behavior of Aluminum/Garnet/Carbon Hybrid Metal Matrix Composites (HMMCs) Fabricated by Chill Casting Method. *J. Mater. Sci. Chem. Eng.* **2015**, *3*, 1–8. [[CrossRef](#)]
74. Moona, G.; Walia, R.S.; Rastogi, V.; Sharma, R. Aluminium Metal Matrix Composites: A Retrospective Investigation. *Indian J. Pure Appl. Phys.* **2018**, *56*, 164–175.
75. Su, H.; Gao, W.; Feng, Z.; Lu, Z. Processing, microstructure and tensile properties of nano-sized Al₂O₃ particle reinforced aluminum matrix composites. *Mater. Des.* **2012**, *36*, 590–596. [[CrossRef](#)]
76. Contreras, A.; López, V.H.; Bedolla, E. Mg/TiC composites manufactured by pressureless melt infiltration. *Scr. Mater.* **2004**, *51*, 249–253. [[CrossRef](#)]
77. Batchelor, G. *An Introduction to Fluid Dynamics*; Cambridge University Press: Cambridge, UK, 1967.
78. Khanafer, K.; Vafai, K. A Critical Synthesis of Thermophysical Characteristics of Nanofluids. In *Nanotechnology and Energy*; Jenny Stanford Publishing: Singapore, 2017; pp. 279–332. [[CrossRef](#)]
79. Lin, Y.; Kang, K.; Chen, F.; Zhang, L.; Lavernia, E.J. Gradient Metal Matrix Composites. *Compr. Compos. Mater. II* **2018**, *4*, 331–346. [[CrossRef](#)]
80. Contreras Cuevas, A.; Bedolla Becerril, E.; Martínez, M.S.; Lemus Ruiz, J. Fabrication Processes for Metal Matrix Composites. *Met. Matrix Compos.* **2018**, 83–114. [[CrossRef](#)] [[PubMed](#)]
81. Amosov, A.P.; Latukhin, E.I.; Umerov, E.R. Applying Infiltration Processes and Self-Propagating High-Temperature Synthesis for Manufacturing Cermets: A Review. *Russ. J. Non-Ferr. Met.* **2022**, *63*, 81–100. [[CrossRef](#)]
82. Etemadi, R.; Wang, B.; Pillai, K.M.; Niroumand, B.; Omrani, E.; Rohatgi, P. Pressure infiltration processes to synthesize metal matrix composites—A review of metal matrix composites, the technology and process simulation. *Mater. Manuf. Process.* **2018**, *33*, 1261–1290. [[CrossRef](#)]
83. Long, S.; Beffort, O.; Uzwil, G.M.; Thevoz, P. Processing of Al-based MMCs by indirect squeeze infiltration of ceramic preforms on a shot-control high pressure die casting machine. *Aluminium* **2000**, *76*, 82–89.
84. Amosov, A.P.; Fedotov, A.F.; Latukhin, E.I.; Novikov, V.A. TiC–Al interpenetrating composites by SHS pressing. *Int. J. Self-Propagating High-Temp. Synth.* **2015**, *24*, 187–191.
85. Fedotov, A.F.; Amosov, A.P.; Latukhin, E.I.; Novikov, V.A. Fabrication of aluminum–ceramic skeleton composites based on the Ti₂AlC MAX phase by SHS compaction. *Russ. J. Non-Ferrous Met.* **2016**, *57*, 33–40.
86. Amosov, A.P.; Latukhin, E.I.; Ryabov, A.M.; Umerov, E.R.; Novikov, V.A. Application of SHS process for fabrication of copper-titanium silicon carbide composite (Cu-Ti₃SiC₂). *J. Phys. Conf. Ser.* **2018**, *1115*, 042003. [[CrossRef](#)]
87. Amosov, A.P.; Latukhin, E.I.; Ryabov, A.M. Applying SHS for the Fabrication of the Ti₃SiC₂–Ni Composite. *Russ. J. Non-Ferr. Met.* **2019**, *60*, 555–565.
88. Chadwick, G.A. Squeeze casting of metal matrix composites using short fibre preforms. *Mater. Sci. Eng. A* **1991**, *135*, 23–28. [[CrossRef](#)]
89. Zantout, B.; Das, A.; Franklin, J. Squeeze-Cast Aluminum-Matrix Composite: Strength. In Proceedings of the Metallurgy of Light Alloys: Spring Residential Conference, Loughborough, UK, March 1983.
90. Yue, T.M.; Dai, Y.; Lau, W.S. An Examination of Wire Electrical Discharge Machining (WEDM) of Al₂O₃ Particulate Reinforced Aluminum Based Composites. *Mater. Manuf. Process* **1996**, *11*, 341–350. [[CrossRef](#)]
91. Schultz, B.F.; Ferguson, J.B.; Rohatgi, P.K. Microstructure and hardness of Al₂O₃ nanoparticle reinforced Al–Mg composites fabricated by reactive wetting and stir mixing. *Mater. Sci. Eng. A* **2011**, *530*, 87–97. [[CrossRef](#)]
92. Kainer, K.U. *Metal Matrix Composites: Custom-Made Materials for Automotive and Aerospace Engineering*; Wiley: Hoboken, NJ, USA, 2006; pp. 1–314. [[CrossRef](#)]
93. Metal, V.I.O.A.L. Casting particulate and fibrous metal-matrix composites. In *Composites, Corrosion/Coating of Advanced Materials*; Ikebukuro: Tokyo, Japan, 1989; p. 35.
94. Michaud, V. Liquid-State Processing (of Metal Matrix Composites). In *Fundamentals of Metal-Matrix Composites*; Butterworth-Heinemann: Stoneham, MA, USA, 1993; pp. 3–22.
95. ASM. *ASM Handbook: Alloy Phase Diagrams*; ASM International: Detroit, MI, USA, 1992.
96. Hajjari, E.; Divandari, M.; Arabi, H. Effect of Applied Pressure and Nickel Coating on Microstructural Development in Continuous Carbon Fiber-Reinforced Aluminum Composites Fabricated by Squeeze Casting. *Mater. Manuf. Process.* **2011**, *26*, 599–603. [[CrossRef](#)]
97. Chung, W.S.; Lin, S.J. Ni-coated SiC_p reinforced aluminum composites processed by vacuum infiltration. *Mater. Res. Bull.* **1996**, *31*, 1437–1447. [[CrossRef](#)]
98. Sree Manu, K.M.; Ajay Raag, L.; Rajan, T.P.D.; Gupta, M.; Pai, B.C. Liquid Metal Infiltration Processing of Metallic Composites: A Critical Review. *Metall. Mater. Trans. B* **2016**, *47*, 2799–2819. [[CrossRef](#)]
99. Andrews, R.M.; Mortensen, A. Lorentz force infiltration of fibrous preforms. *Metall. Trans. A* **1991**, *22*, 2903–2915.

100. Saberi, Y.; Zebarjad, S.M.; Akbari, G.H. On the role of nano-size SiC on lattice strain and grain size of Al/SiC nanocomposite. *J. Alloys Compd.* **2009**, *484*, 637–640. [CrossRef]
101. Wannasin, J.; Flemings, M.C. Fabrication of metal matrix composites by a high-pressure centrifugal infiltration process. *J. Mater. Process. Technol.* **2005**, *169*, 143–149. [CrossRef]
102. Nishida, Y.; Izawa, N.; Kuramasu, Y. Recycling of aluminum matrix composites. *Metall. Mater. Trans. A Phys. Metall. Mater. Sci.* **1999**, *30*, 839–844.
103. Sahin, Y.; Acilar, M. Production and properties of SiC_p-reinforced aluminium alloy composites. *Compos. Part A Appl. Sci. Manuf.* **2003**, *34*, 709–718. [CrossRef]
104. Terry, B.; Jones, G. Metal Matrix Composites: Current Developments and Future Trends in Industrial Research and Applications. Available online: <https://cir.nii.ac.jp/crid/1130282270262518272> (accessed on 19 March 2024).
105. Kumar, S.; Chakraborty, M.; Subramanya Sarma, V.; Murty, B.S. Tensile and wear behaviour of in situ Al-7Si/TiB₂ particulate composites. *Wear* **2008**, *265*, 134–142. [CrossRef]
106. Mandal, A.; Chakraborty, M.; Murty, B.S. Ageing behaviour of A356 alloy reinforced with in-situ formed TiB₂ particles. *Mater. Sci. Eng. A* **2008**, *489*, 220–226. [CrossRef]
107. Zhang, Y.; Ma, N.; Wang, H.; Le, Y.; Li, X. Damping capacity of in situ TiB₂ particulates reinforced aluminium composites with Ti addition. *Mater. Des.* **2007**, *28*, 628–632. [CrossRef]
108. Zhang, Y.; Ma, N.; Wang, H. Effect of particulate/Al interface on the damping behavior of in situ TiB₂ reinforced aluminium composite. *Mater. Lett.* **2007**, *61*, 3273–3275. [CrossRef]
109. Pramod, S.L.; Bakshi, S.R.; Murty, B.S. Aluminum-Based Cast In Situ Composites: A Review. *J. Mater. Eng. Perform.* **2015**, *24*, 2185–2207.
110. Niranjan, K.; Lakshminarayanan, P.R. Dry sliding wear behaviour of in situ Al-TiB₂ composites. *Mater. Des.* **2013**, *47*, 167–173. [CrossRef]
111. Murty, B.S.; Maiti, R.; Chakraborty, M. Development of in-situ Al-TiB₂ Metal Matrix Composites. *J. Metall. Mater. Sci.* **2001**, *43*, 93–101.
112. Yang, B.; Wang, Y.Q.; Zhou, B.L. The mechanism of formation of TiB₂ particulates prepared by in situ reaction in molten aluminum. *Metall. Mater. Trans. B Process Metall. Mater. Process. Sci.* **1998**, *29*, 635–640.
113. Tee, K.L.; Lu, L.; Lai, M.O. In situ processing of Al-TiB₂ composite by the stir-casting technique. *J. Mater. Process. Technol.* **1999**, *89–90*, 513–519. [CrossRef]
114. Patel, N.S.; Patel, A.D. Studies on Properties of Composite Material (Al-SiC MMC) for Valve Development of Light Vehicle Petrol Engine—A Technical Research. *GRD J.-Glob. Res. Dev. J. Eng.* **2017**, *2*.
115. Amosov, A.P.; Luts, A.R.; Rybakov, A.D.; Latukhin, E.I. Using Different Powdered Carbon Forms for Reinforcing Aluminum Composite Materials with Carbon and Titanium Carbide: A Review. *Russ. J. Non-Ferr. Met.* **2020**, *61*, 500–516. [PubMed]
116. Song, S.G.; Shi, N.; Gray, G.T.; Roberts, J.A. Reinforcement shape effects on the fracture behavior and ductility of particulate-reinforced 6061-Al matrix composites. *Metall. Mater. Trans. A Phys. Metall. Mater. Sci.* **1996**, *27*, 3739–3746.
117. Yang, Z.; Fan, J.; Liu, Y.; Nie, J.; Yang, Z.; Kang, Y. Effect of the Particle Size and Matrix Strength on Strengthening and Damage Process of the Particle Reinforced Metal Matrix Composites. *Materials* **2021**, *14*, 675. [CrossRef] [PubMed]
118. El-Kady, O.; Fathy, A. Effect of SiC particle size on the physical and mechanical properties of extruded Al matrix nanocomposites. *Mater. Des.* **2014**, *54*, 348–353. [CrossRef]
119. Li, Y.; Ramesh, K.T. Influence of particle volume fraction, shape, and aspect ratio on the behavior of particle-reinforced metal-matrix composites at high rates of strain. *Acta Mater.* **1998**, *46*, 5633–5646. [CrossRef]
120. Lewis, C.A.; Withers, P.J. Weibull modelling of particle cracking in metal matrix composites. *Acta Metall. Mater.* **1995**, *43*, 3685–3699. [CrossRef]
121. Chawla, K.K. Metal Matrix Composites. *Compos. Mater.* **1998**, 164–211. [CrossRef] [PubMed]
122. Xia, Z.; Curtin, W.A.; Peters, P.W.M. Multiscale modeling of failure in metal matrix composites. *Acta Mater.* **2001**, *49*, 273–287. [CrossRef]
123. Weissenbek, E.; Böhm, H.J.; Rammerstorfer, F.G. Micromechanical investigations of arrangement effects in particle reinforced metal matrix composites. *Comput. Mater. Sci.* **1994**, *3*, 263–278. [CrossRef]
124. Christman, T.; Needleman, A.; Nutt, S.; Suresh, S. On microstructural evolution and micromechanical modelling of deformation of a whisker-reinforced metal-matrix composite. *Mater. Sci. Eng. A* **1989**, *107*, 49–61. [CrossRef]
125. Tvergaard, V. Analysis of tensile properties for a whisker-reinforced metal-matrix composite. *Acta Metall. Mater.* **1990**, *38*, 185–194. [CrossRef]
126. Lloyd, D.J. Particle reinforced aluminium and magnesium matrix composites. *Int. Mater. Rev.* **2013**, *39*, 1–23. [CrossRef]
127. Hunt, W.H.; Osman, T.M.; Lewandowski, J.J. Micro- and macrostructural factors in DRA fracture resistance. *JOM* **1993**, *45*, 30–35.
128. Bauri, R.; Yadav, D. Metal Matrix Composites by Friction Stir Processing. Available online: https://books.google.co.in/books?hl=en&lr=&id=AMkpDwAAQBAJ&oi=fnd&pg=PP1&dq=Introduction+to+Metal+Matrix+Composites+R.+Bauri&ots=9SADEZbBVy&sig=Hzr52zh_qiC51qS77fP3G6gndqg&redir_esc=y#v=onepage&q=Introduction%20to%20Metal%20Matrix%20Composites+R.%20Bauri&f=false (accessed on 27 March 2024).
129. Hunt, W.H.; Miracle, D.B. Automotive Applications of Metal-Matrix Composites. In *Composites*; ASM International: Detroit, MI, USA, 2001; pp. 1029–1032. [CrossRef]

130. Miracle, D.B. Aeronautical Applications of Metal-Matrix Composites. In *Composites*; ASM International: Detroit, MI, USA, 2001; pp. 1043–1049. [[CrossRef](#)]
131. Miracle, D.B.; Donaldson, S.L.; Henry, S.D.; Moosbrugger, C.; Anton, G.J.; Sanders, B.R.; Hrivnak, N.; Terman, C.; Kinson, J.; Muldoon, K.; et al. *ASM Handbook*; ASM International: Materials Park, OH, USA, 2001; ISBN 9780871707031.

Disclaimer/Publisher’s Note: The statements, opinions and data contained in all publications are solely those of the individual author(s) and contributor(s) and not of MDPI and/or the editor(s). MDPI and/or the editor(s) disclaim responsibility for any injury to people or property resulting from any ideas, methods, instructions or products referred to in the content.